Computationally Efficient MIMO HSDPA System-Level Modeling

Martin Wrulich, [Aff1]
Corresponding Affiliation: Aff1
Email: mwrulich@nt.tuwien.ac.at

Markus Rupp, [Aff1]
Email: mrupp@nt.tuwien.ac.at

Aff1 Institute of Communications and Radio Frequency Engineering, Vienna University of Technology, 1040 Vienna, Austria

Abstract

Multiple-input multiple-output (MIMO) techniques are regarded as the crucial enhancement of todays wireless access technologies to allow for a significant increase in spectral efficiency. After intensive research on single link performance, the third Generation Partnership Project (3GPP) integrated a spatial multiplexing scheme as MIMO extension of High-Speed Downlink Packet Access (HSDPA). Despite the scientific findings on the link-level performance of MIMO techniques, many questions relevant for the design and optimization of cellular networks remain

unanswered. In particular, it has to be identified whether, and to which amount, the predicted MIMO link-level performance gains can be achieved in an entire network. In this paper, we present a computationally efficient link-to-system level model for system-level evaluations of MIMO HSDPA and an exemplary embedding in a MATLAB-based system-level simulator. The introduced equivalent fading parameter structure allows for a semianalytic physical-layer abstraction with high prediction accuracy and simultaneous moderate complexity.

1. Introduction

Mobile radio communication represents one of the most persistent growing technology markets since the introduction of the Global System for Mobile communications (GSM). Todays cellular networks utilized by mobile network operators are based on the Wideband Code-Division Multiple Access (W-CDMA) transmission standard. To satisfy the demand for high data rate in cellular mobile communication systems, spectral efficiency has to be increased. Accordingly, MIMO techniques have been in focus of research for several years now and 3GPP has considered numerous proposals for the MIMO enhancement of Frequency Division Duplex (FDD) HSDPA [1]. In late 2006, 3GPP decided in favor of Double Transmit Antenna Array (D-TxAA) to be the next evolutionary step of the classical Single-Input Single-Output (SISO) HSDPA [2]. For commercial deployments, large numbers of antennas at the mobile terminal are usually not desired due to limited space and battery capacity, as well as cost arguments. D-TxAA offers the flexibility to exploit MIMO gains and tries to benefit from channel quality adaptability by means of closed loop feedback.

Usually, link-level simulations are a means to identify and evaluate promising transmission techniques. Whereas these investigations are suitable for the development of receiver algorithms, feedback strategies, coding design, and so on, they are not capable of reflecting network issues like cell planning, scheduling, and interference situations in the context of massive multiuser operation. Therefore, to understand system and user performance under reasonable operating conditions in various deployment scenarios, system-level simulations are crucial [3–5]. These simulations try to cover at least

(1) network deployment issues including network performance [6–8],

(2) multiuser and multibase-station (intercell) interference [9–11],

(3) Radio Link Control (RLC) and admission control algorithms [12, 13],

(4) scheduling [14, 15].

One of the major difficulties of system-level analyses is the computational complexity involved in

evaluating the performance of the radio links between all base-stations and mobile terminals. Performing such a large number of link-level simulations is clearly prohibitive. Thus, those evaluations have to rely on simplified link models that still must be accurate enough to capture the essential behavior [16–21]. Generally speaking, for system-level evaluations, two concatenated models are needed. The so-called *link-measurement model* represents the measurements for link adaption and resource allocation. Constitutive, the *link-performance model* grants a possibility to determine the BLock Error Ratio (BLER) given a certain resource and power allocation as well as signal processing. Both models are related in the sense that they provide figures of performance prediction and together can be referred to as *system-level interface* [22, 23]. A schematic overview of the relations and dependencies on system level is illustrated in Figure 1.

Figure 1 Schematic block diagram of relations on system level [23].
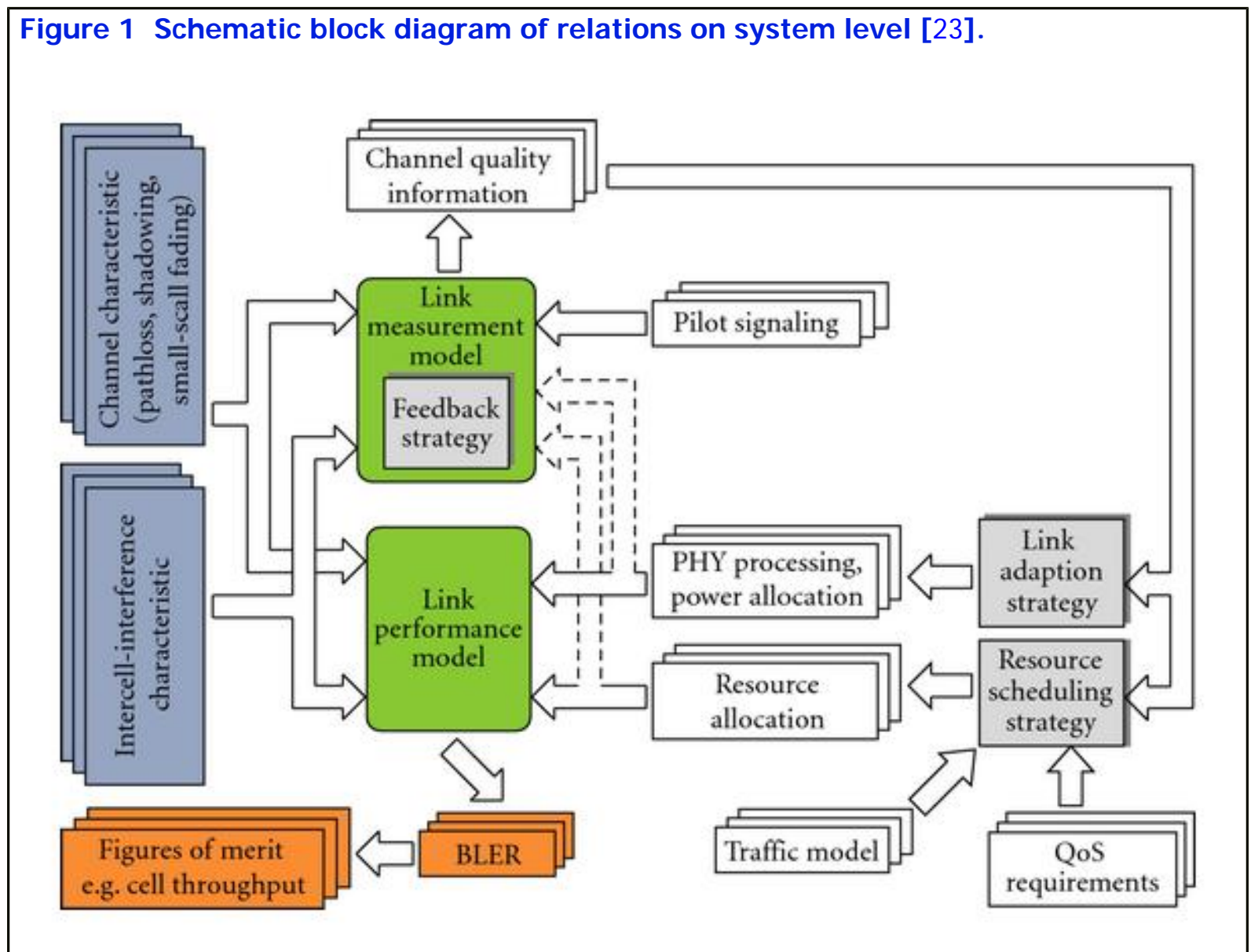
In order to enable a comparison of a large variety of system realizations, it is desirable to have

measurement and performance models that are general enough to cover different multiple access strategies and transceiver types, including multiple antenna techniques such as precoding and spatial multiplexing. It should also be possible to derive the parameters of such a model from a limited number of link-level simulations. This means that the model should ideally cover channel and interference conditions beyond those used for training. The existing system level models for SISO W-CDMA systems, see, for example, [3, 24], cannot be used in a straightforward way for MIMO-enhanced systems, and none of the published works accurately model the proposed D-TxAA transmission scheme so far. Either the utilization of Minimum Mean Squared Error (MMSE) equalizers is not supported (as recommended for MIMO HSDPA) [17, 25], multiple-stream operation is not covered [13], the mandatory precoding (e.g., for D-TxAA) is missing [24], or no full analytical description is derived to be available for system-level evaluations [12, 13]. Furthermore, all of the cited works need to compute the full complex-valued MIMO channel matrix on system level, which—together with the necessary complex multiplications, the evaluation of the precoding and the equalizer coefficients—implies a large computational burden on system level.

In this paper, we propose a computationally efficient link-to-system level model for the semianalytical physical-layer abstraction. We provide a complete analytical description of the postequalization symbol-level signal-to-inference-and-noise ratio (SINR) including the precoding, spreading/despreading, and MMSE equalization. Our model shows a structure that identifies the relevant interference terms—which enables, for example, receiver optimizations [26, 27]—and allows for the generation of scalar *fading parameters* prior to the system-level simulation. Utilizing this special structure, nearly all link-dedicated procedures can be included in these fading parameters, thus during the runtime of the system-level simulation only scalar multiplications are needed to compute the SINR. This *significantly* reduces the computational effort. In principle, this idea has already been touched in [18] for Universal Mobile Telecommunications System (UMTS) W-CDMA, however, in the context of MIMO, we need to generalize and fairly extend it to be able to derive a suitable description. Furthermore, we will elaborate our modeling of the link-performance (BLER). To summarize, our contributions in this article are
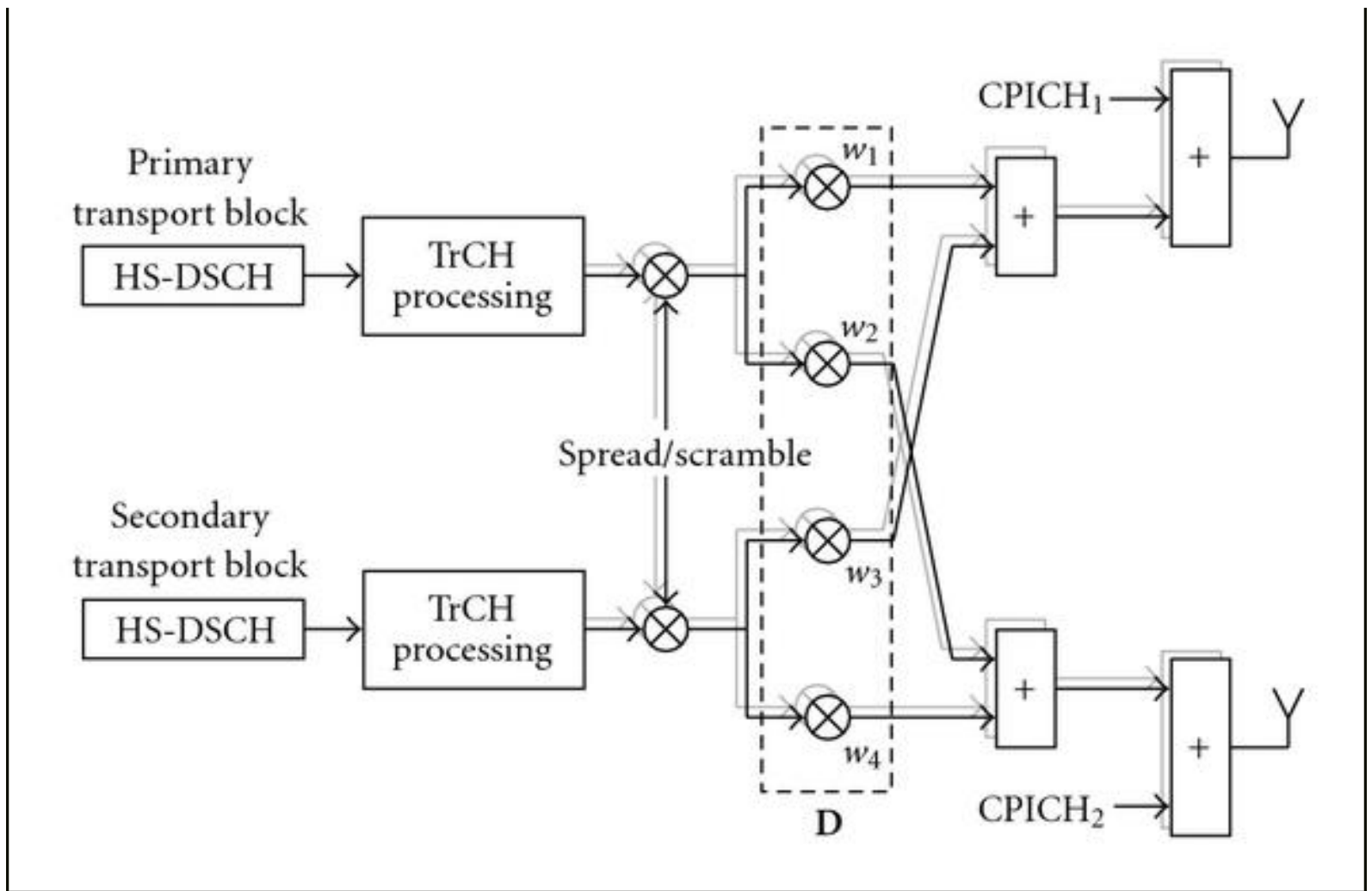
(i) a computationally efficient *link-to-system level model* capable of accurately representing the D-TxAA physical layer,

(ii) an exemplary *system-level simulator* concept based on the proposed modeling.

The paper is organized as follows: in Section 2, we describe the basic concept of D-TxAA MIMO HSDPA. Consequently, we derive our proposed computationally efficient link-measurement model in Sections 3 and 4, then explain the employed link-performance model, after which we introduce a possible implementation concept of a system-level simulator in Section 5. Finally, Section 6 concludes this paper.

2. D-TxAA

The Radio Access Network (RAN) group agreed to standardize MIMO in HSDPA for UMTS Terrestrial Radio Access (UTRA) frequency division duplex as dual-codeword MIMO based on D-TxAA with the weights applied on the transmitter side being signalled on the High-Speed Shared Control CHannel (HS-SCCH) in the downlink. The focus of this scheme is aimed at two transmit and two receive antennas. A high level description of the D-TxAA scheme is depicted in Figure 2, see also [1]. Channel coding, interleaving, and spreading are implemented as in the non-MIMO mode, with a *primary transport block* being always present. However, now the physical layer supports the transport of a *secondary transport block* to a User Equipment (UE) within one Transmission Time Interval (TTI). The precoding weights for the transmit antenna array operation are determined from a quantized set by the UE and serve as beamforming to maximize the received SINR. In case of a single-stream transmission, the primary precoding vector, determined by $[w_1, w_2]^T$, is used for the transmission of the primary transport block. In a dual stream transmission, the secondary precoding vector $[w_3, w_4]^T$ is chosen orthogonal to the primary one which keeps the amount of feedback bits constant for both transmission modes. The evaluated feedback in form of the Precoding Control Information (PCI) is fed back to the Node-B within a composite Channel Quality Indicator (CQI)/ PCI report on the High-Speed Downlink Physical Control CHannel (HS-DPCCH). This scheme theoretically allows for a doubled data rate compared to the actual possible HSDPA data rates [28] which can be utilized in high SINR regions (e.g., very close to the serving Node-B) when dual stream mode is supported.

Figure 2 High level description of the D-TxAA transmission scheme. The precoding weights $w_1, \ldots, w_4$ are signaled by the UE.

3. Computationally Efficient Link-Measurement Model

To be able to derive an accurate and computationally efficient system-level model, an analytical model of the W-CDMA MIMO HSDPA [1] link quality is required. Therefore, we adapted the framework of [29] in order to reflect one individual link between a base station and a user equipment.

Figure 3 depicts the model where the transmitter (Tx) and the receiver (Rx) are equipped with n_T and n_R antennas, respectively. Note that this description allows for the description of more than two spatial multiplexed data streams. Accordingly, as illustrated in Figure 3, the input data stream s is demultiplexed into N parallel streams, $s_0, \dots, s_{N-1}$, with the individual data streams s_n, $0 \le n \le N-1$, being spread by a number of spreading sequences, φ_n (multicode usage) and scrambling sequences (not depicted in Figure 3). In a practical HSDPA system, however, the Node-B will most probably use only one scrambling code.

Figure 3 System model for a W-CDMA system, reflecting the parallel transmission of N streams over n_T transmit antennas and reception with n_R receive antennas by using an ST-MMSE.
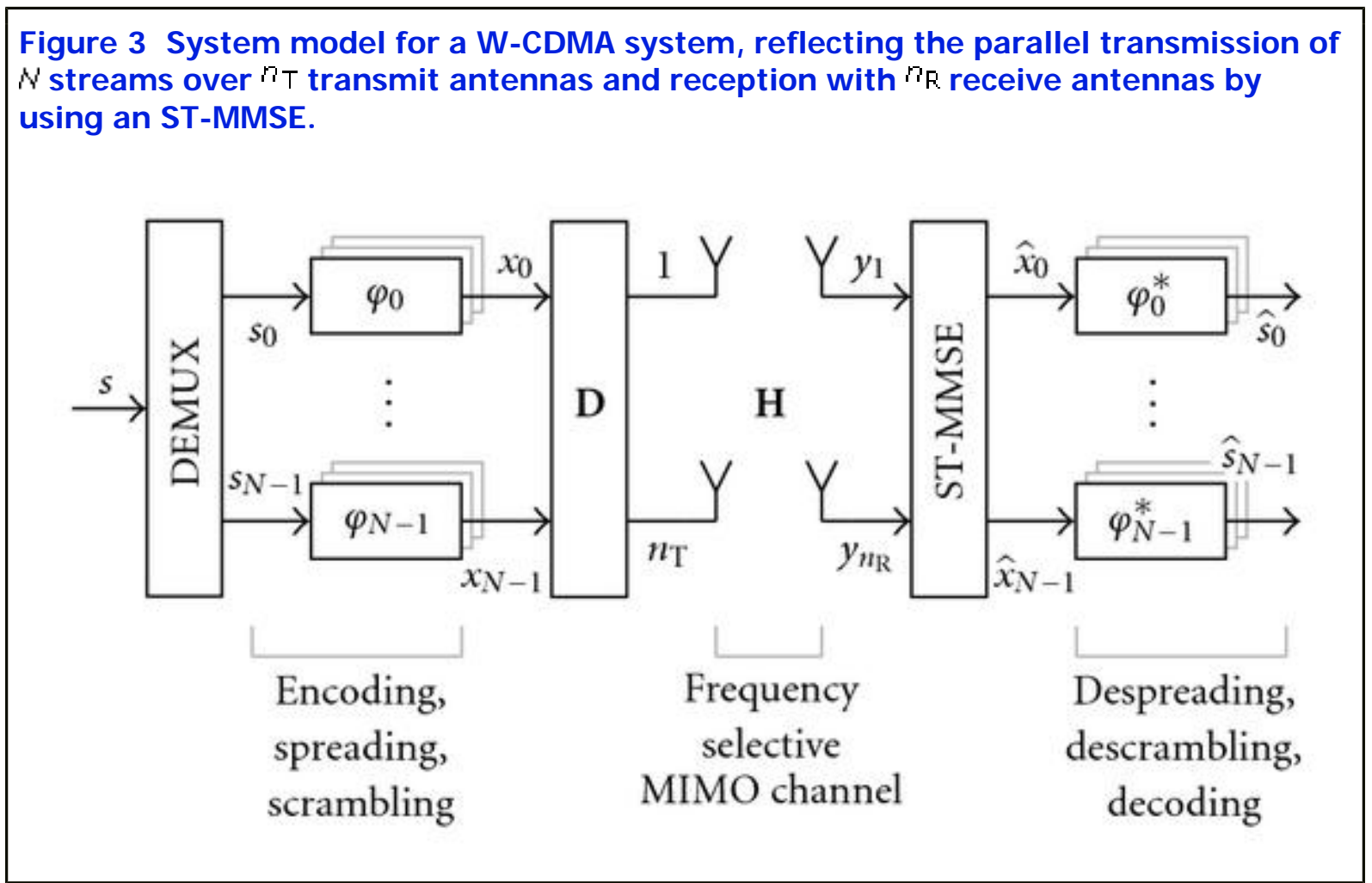
These spread and scrambled sequences are then mapped to the n_T transmit antennas using a prefiltering matrix $\mathbf{D} \in \mathbb{C}^{n_T \times N}$, which contains the precoding weights, $w_1, \ldots, w_{n_T N}$, like depicted in Figure 2. At the receiver, the signals are gathered with n_R antennas and chip-spaced sampled before they enter the discrete time Space-Time MMSE (ST-MMSE) equalizer. The MIMO channel $\mathbf{H} \in \mathbb{C}^{n_R \times n_T L}$ is modeled as time-discrete, frequency-selective channel:

$$\mathbf{H} = \begin{bmatrix} h_{1,1}(0) & \cdots & h_{1,n_T}(0) & \cdots & h_{1,n_T}(L-1) \\ \vdots & \vdots & \vdots & \ddots & \vdots \\ h_{n_R,1}(0) & \cdots & h_{n_R,n_T}(0) & \cdots & h_{n_R,n_T}(L-1) \end{bmatrix}, \tag{1}$$

where the entry $h_{r,t}(l)$ denotes the lth sampled chip of the channel impulse response from transmit antenna t to receive antenna r, with a total length of L chip intervals. Note that the pulse shaping, the transmit and receive filtering, as well as the sampling operation can be incorporated in the MIMO channel matrix.

For sake of notational simplicity, we define an equivalent time discrete channel $\Gamma \in \mathbb{C}^{n_R \times NL}$ that

includes the prefiltering matrix $\mathbf{D}$ and the MIMO channel $\mathbf{H}$, that is, $\Gamma = \mathbf{H} \cdot (\mathbf{I}_L \otimes \mathbf{D})$, with $\mathbf{I}_L$ denoting the identity matrix of size L, and $\otimes$ being the Kronecker product. With this, the input output relation at time instant k, formulated by means of the equivalent channel matrix, is given by $\mathbf{y}(k) = \Gamma \mathbf{x}(k) + \mathbf{n}(k)$, where we introduced the receive vector $\mathbf{y}(k) = [y_1(k), \dots, y_{n_R}(k)]^T$, the transmit vector $\mathbf{x}(k) = [x_0(k), \dots, x_{N-1}(k), \dots, x_{N-1}(k - L + 1)]^T$, and the receive noise vector $\mathbf{n}(k) = [n_1(k), \dots, n_{n_R}(k)]^T$. Obviously, this description allows for the representation of the D-TxAA scheme.

3.1. Space-Time MMSE

Since we imply the usage of an ST-MMSE at the receiver, we have to extend our input-output relation for E received samples (the equalizer span) at the n_R receive antennas, that is, $\mathbf{y}_E(k) = \Gamma_E \mathbf{x}_E(k) + \mathbf{n}_E(k)$. The "stacked" versions of the parameters are defined as $\mathbf{y}_E(k) = [\mathbf{y}^T(k), \dots, \mathbf{y}^T(k - E + 1)]^T$, $\mathbf{x}_E(k) = [x_1(k), \dots, x_N(k), \dots, x_N(k - E - L + 2)]^T$, and $\mathbf{n}_E(k) = [\mathbf{n}^T(k), \dots, \mathbf{n}^T(k - E + 1)]^T$, and the equivalent channel matrix $\Gamma_E \in \mathbb{C}^{n_R E \times N \cdot (L + E - 1)}$ is given by

$$
\Gamma_E =
\begin{bmatrix}
\Gamma & \mathbf{0}_{n_R, N} & \cdots & \mathbf{0}_{n_R, N} \\
\mathbf{0}_{n_R, N} & \Gamma & \cdots & \mathbf{0}_{n_R, N} \\
\vdots & \vdots & \ddots & \vdots \\
\mathbf{0}_{n_R, N} & \mathbf{0}_{n_R, N} & \cdots & \Gamma
\end{bmatrix},
\tag{2}
$$

where $\mathbf{0}_{n_R, N}$ denotes the all-zero matrix of dimension $n_R \times N$. Note that this description cannot be represented by a Kronecker product, because Γ_E does not show a block structure, as indicated by the size of the zero matrices $\mathbf{0}_{n_R, N}$.

The solution of this ST-MMSE minimization problem, $\mathbf{W}_d \in \mathbb{C}^{N \times n_R E}$, estimating the data vector $\mathbf{x}_d = \mathbf{x}(k - d) = [x_1(k - d), \dots, x_N(k - d)]^T$ at delay d, can be evaluated to be [29, 30],

$$
\mathbf{W}_d = \mathbf{R}_{\mathbf{x}_d \mathbf{x}_E} \Gamma_E^H \left(\Gamma_E \mathbf{R}_{\mathbf{x}_E \mathbf{x}_E} \Gamma_E^H + \mathbf{R}_{\mathbf{n}_E \mathbf{n}_E} \right)^{-1}.
\tag{3}
$$

The covariance matrices then show the following structure:

$$\mathbf{R}_{\mathbf{x}_d\mathbf{x}_E} = \left[\mathbf{0}_{N\times Nd}, \mathbf{P}, \mathbf{0}_{N\times N(E+L-d+2)}\right],$$ (4)

$$\mathbf{R}_{\mathbf{x}_E\mathbf{x}_E} = \mathrm{diag}_{E+L-1}\{\mathbf{P}\},$$

with $\mathbf{P} = \mathrm{diag}_{i=1,\dots,N}\{P_i\}$ combining the powers P_i, transmitted on the ith stream, respectively.

The equalizer span E and the detection delay d are important parameters that influence the performance of the system, but an optimization of these is not treated in this paper. In general, we assume an equalizer delay of $d = E/2$, according to [31].

3.2. Equivalent Fading Parameters Description

The total received signal at user u can be evaluated by summing over all base-stations B and all users U_b of the bth base-station, respectively, as

$$y(k) = \sum_{b=0}^{B}\sum_{u=0}^{U_b}\sum_{\psi\in\Psi_{ub}}\sum_{\varphi\in\Phi_{ub}}\Gamma_{ub}\mathbf{x}_{ub,\psi,\varphi}(k) + \mathbf{n}_E(k),$$ (5)

where Ψ_{ub} and Φ_{ub} denote the pool of scrambling and spreading codes for user u served by base-station b. The received signal is then passed through the ST-MMSE and—if we omit the noise term for the moment—leads to the useful postequalization signal

$$\hat{x}_n(k) = \sum_{b=0}^{B}\sum_{u=0}^{U_b}\sum_{\psi\in\Psi_{ub}}\sum_{\varphi\in\Phi_{ub}} \sum_{m=0}^{N(E+L-1)-1}\mathbf{w}_n^T\gamma_{ub}^m\mathbf{x}_{ub,\psi,\varphi,\lfloor m/N\rfloor}\left(k - \left\lfloor\frac{m}{N}\right\rfloor\right).$$ (6)

Here, we decomposed $\mathbf{W}_d = [\mathbf{w}_1,\dots,\mathbf{w}_n,\dots,\mathbf{w}_N]^T$ and $\Gamma_{ub} = [\gamma_{ub}^0,\dots,\gamma_{ub}^m,\dots,\gamma_{ub}^{N(E+L-1)-1}]$, where n denotes the stream index and m is the index of the Tx chips for all streams entering the equalizer span. Furthermore, $\lfloor m/N\rfloor$ denotes the largest integer smaller than m/N and represents the delay of the transmit chips, and $\lfloor m/N\rfloor$ denotes the remainder of the integer division and represents the index of the substream.

After the descrambling and despreading, $\hat{x}_n(k)$ is multiplied with the complex conjugated scrambling and spreading codes and integrated over the period of a symbol to obtain the

estimated Tx symbols $\hat{s}_n$. In what follows, let us assume that each Node-B (or cell-sector) uses only one scrambling sequence, thus $\Psi_{ub} = \Psi_b : |\Psi_b| = 1$ whereas each neighboring Node-B uses a different scrambling sequence. This reflects a typical W-CDMA scenario as currently implemented for Release 4 and HSDPA and, accordingly, we will drop the notation of the scrambling sequence where it is possible to simplify the notation. In the following, we will decompose the receive power of $\hat{x}_n(k)$ in (6) into its different interference terms to derive the system level model. With this decomposition, it is possible to describe the characteristics of the individual interference terms by means of *fading-parameters* that are real-valued scalar processes. These parameters can be computed offline and loaded for the runtime of a system-level simulation, thus significantly reducing the computational burden.

3.2.1. Desired Signal

Without losing generality, we define the user and base-station of interest to be $u = 0$ and $b = 0$. Then, the power of the desired signal, $P_{s,n}$, is given by

$$P_{s,n} = \left| \mathbf{w}_n^T \gamma_{00}^{dN+n} \right|^2 \cdot P_{n,\zeta} = G_{s,n} \cdot P_{n,\zeta} \tag{7}$$

where $P_{n,\zeta}$ denotes the power on stream n and spreading code ζ spent for user $u = 0$ by base-station $b = 0$. The fading parameter $G_{s,n} \triangleq \left| \mathbf{w}_n^T \gamma_{00}^{dN+n} \right|^2$ describes the equivalent fading of the useful signal power.

3.2.2. Intracell Interference

The intracell interference is composed by a number of terms, that is, the remaining intersymbol interference (ISI) after equalization, $P_{ISI,n}$, the intercode interference when the same scrambling but a different spreading code is used, $P_{IC,n}$, the intracell interference from users that are not served in the same instant as the user of interest but with the same scrambling and spreading code, $P_{intra_1,n}$, and the intracell interference from users with the same scrambling but different spreading code, $P_{intra_2,n}$. From these terms, $P_{ISI,n}$ and $P_{IC,n}$ represent the intracell interference generated by the user of interest (selfinterference):

$$P_{\text{ISI},n} + P_{\text{IC},n} = \sum_{\substack{m=0 \\ m \notin [dN, dN+N-1]}}^{N(E+L-1)-1} \left| \mathbf{w}_n^T \mathbf{r}_{00}^m \right|^2 P_{0,\lfloor m/N \rfloor}, \tag{8}$$

and $P_{\text{intra}_1,n}$ together with $P_{\text{intra}_2,n}$ specify the intracell interference generated by all other users in the cell:

$$P_{\text{intra}_1,n} + P_{\text{intra}_2,n} = \sum_{u=1}^{U_0} \sum_{\substack{m=0 \\ m \notin [dN, dN+N-1]}}^{N(E+L-1)-1} \left| \mathbf{w}_n^T \mathbf{r}_{u0}^m \right|^2 P_{u,\lfloor m/N \rfloor}, \tag{9}$$

where we defined $P_{u,\lfloor m/N \rfloor}$ to be the user specific power spent by base-station $b = 0$ on substream $\lfloor m/N \rfloor$. If we apply the simplification that all streams designated for a user u has the same power P_u, the total intracell interference becomes

$$P_{\text{intra},n} = \underbrace{\frac{1}{N}P_0 \sum_{\substack{m=0 \\ m \notin [dN, dN+N-1]}}^{N(E+L-1)-1} \left| \mathbf{w}_n^T \mathbf{r}_{00}^m \right|^2}_{\text{from user of interest}} + \underbrace{\frac{1}{N}\sum_{u=1}^{U_0} P_u \sum_{\substack{m=0 \\ m \notin [dN, dN+N-1]}}^{N(E+L-1)-1} \left| \mathbf{w}_n^T \mathbf{r}_{u0}^m \right|^2}_{\text{from other users in the cell}}, \tag{10}$$

with $P_u = \sum_{n=0}^{N-1} P_{u,n}$. So far, the description of (10) does not allow for a decoupling into fading parameters and power terms because $\mathbf{r}_{u0}^m$ depends on the user index, that is, the choice of the user regarding their precoding, which is only known on system level. To be able to decompose it, we have to introduce another simplification, namely, to replace $\sum_{\substack{m=0 \\ m \notin [dN, dN+N-1]}}^{N(E+L-1)-1} \left| \mathbf{w}_n^T \mathbf{r}_{u0}^m \right|^2$ by an average over the precoding choices of the users. If we assume a uniform utilization of all precoding vector choices, the resulting term becomes

$$\frac{1}{|\Omega|} \sum_{\omega \in \Omega} \sum_{\substack{m=0 \\ m \notin [dN, dN+N-1]}}^{N(E+L-1)-1} \left| \mathbf{w}_n^T \mathbf{r}_{\mathbf{w}0}^m \right|^2, \tag{11}$$

with ω denoting the precoding choice out of the code-book Ω. The vector $\mathbf{r}_{\mathbf{w}0}^m$ denotes the channel matrix column m when applying precoding vector $\mathbf{w}$ at the transmitter side. Due to this averaging, (11) does not depend on the user index anymore. By normalization with respect to the useful signal power $G_{s,n}$, we define the precoding orthogonality:

$$o_{BF,n} \triangleq \frac{1}{G_{s,n}} \frac{1}{|\Omega|} \sum_{\omega \in \Omega} \sum_{\substack{m=0 \\ m \notin [dN, dN+N-1]}}^{N(E+L-1)-1} \left| \mathbf{w}_n^T \mathbf{r}_{\mathbf{w}0}^m \right|^2, \tag{12}$$

characterizing the ability of the equalizer to cancel interference caused by multiuser scheduling.

With this simplification, we can represent the intracell interference affecting stream n by

$$P_{intra,n} = \left[P_0 + o_{BF,n} \cdot \sum_{u=1}^{U_0} P_u \right] o_{intra,n} \cdot G_{s,n}, \tag{13}$$

with the intracell orthogonality fading, $o_{intra,n}$, being

$$o_{intra,n} \triangleq \frac{1}{N} \cdot \frac{\sum_{\substack{m=0 \\ m \notin [dN, dN+N-1]}}^{N(E+L-1)-1} \left| \mathbf{w}_n^T \mathbf{r}_{00}^m \right|^2}{\left| \mathbf{w}_n^T \mathbf{r}_{00}^{dN+n} \right|^2}. \tag{14}$$

3.2.3. Intrastream Interference

The interference generated by the parallel transmission of a second (spatially multiplexed) stream is given by the power $P_{INT,n}$, and can be expressed as

$$P_{INT,n} = \sum_{\substack{m=0 \\ m \neq n}}^{N-1} \left| \mathbf{w}_n^T \mathbf{\gamma}_{00}^{dN+m} \right|^2 \cdot P_{m,\zeta}$$

$$= G_{s,n} \cdot \sum_{\substack{m=0 \\ m \neq n}}^{N-1} o_{INT,m} \cdot P_{m,\zeta},$$

(15)

where $o_{INT,m} \triangleq \left| \mathbf{w}_n^T \mathbf{\gamma}_{00}^{dN+m} \right|^2$ denotes the intrastream orthogonality factor.

3.2.4. Intercell Interference

For this interference term, we will assume that all users in a neighbouring cell will apply the same precoding coefficients. If we, furthermore, restrict ourselves to the scenario that all substreams designated for one user are equally powered, the intercell interference is given by

$$P_{inter,n} = \sum_{b=1}^{B} P_{tot,b} \frac{1}{N} \mathbf{w}_n^T \left[\sum_{m=0}^{N(E+L-1)-1} \mathbf{\gamma}_{0b}^m \left(\mathbf{\gamma}_{0b}^m \right)^H \right] \mathbf{w}_n^*$$

$$= \sum_{b=1}^{B} P_{tot,b} \, G_{inter,b,n},$$

(16)

where $P_{tot,b}$ denotes the total transmit power of Node-B b spent for the HSDPA data transmission to all served users, and $G_{inter,b,n}$ is the equivalent intercell fading process.

To confirm the validity of our main assumption, that is, the application of equal precoding coefficients for all users, we performed some simulations to investigate the effect of this simplified modeling onto the intercell interference. For these simulations, we assumed equal powers on all streams, and equal powers for all active users, which is likely to be set in a realistic network deployment. Furthermore, we only evaluated the intercell interference of one neighbouring Node-B because the interference arriving from one specific neighbouring Node-B will be independent of all other neighbouring Node-Bs due to the fact that the small-scale fading of their corresponding channels (to the desired user) can be assumed independent of each other.

Hence, to assess the approximation error, we simulated the intercell interference power, as given in (16) for two cases: all users are served with random precoding vectors (PC = rand) and the simplified version, in which all users are served with one specific, constant precoding vector (PC = 1).

Figure 4 shows the simulation results for both cases when the channel is modeled as Rayleigh fading in a 2×2 MIMO channel with International Telecommunication Union (ITU) PedA profile, [32–34]. It can be seen that the Cumulative Density Function (cdfs) of $P_{inter,n}$ for the random and the fixed precoding assignment are identical, thus there is no error introduced by our simplification. The reason for this is that the precoding gain vanishes in the double-stream operation, as shown in Section 3.1. In the single-stream mode the proposed simplification introduces an insignificant error, but the results are left out due to limited space.

Figure 4 Cdfs of the intercell interference power $P_{inter,n}$ in case of a 2×2 ITU PedA channel.
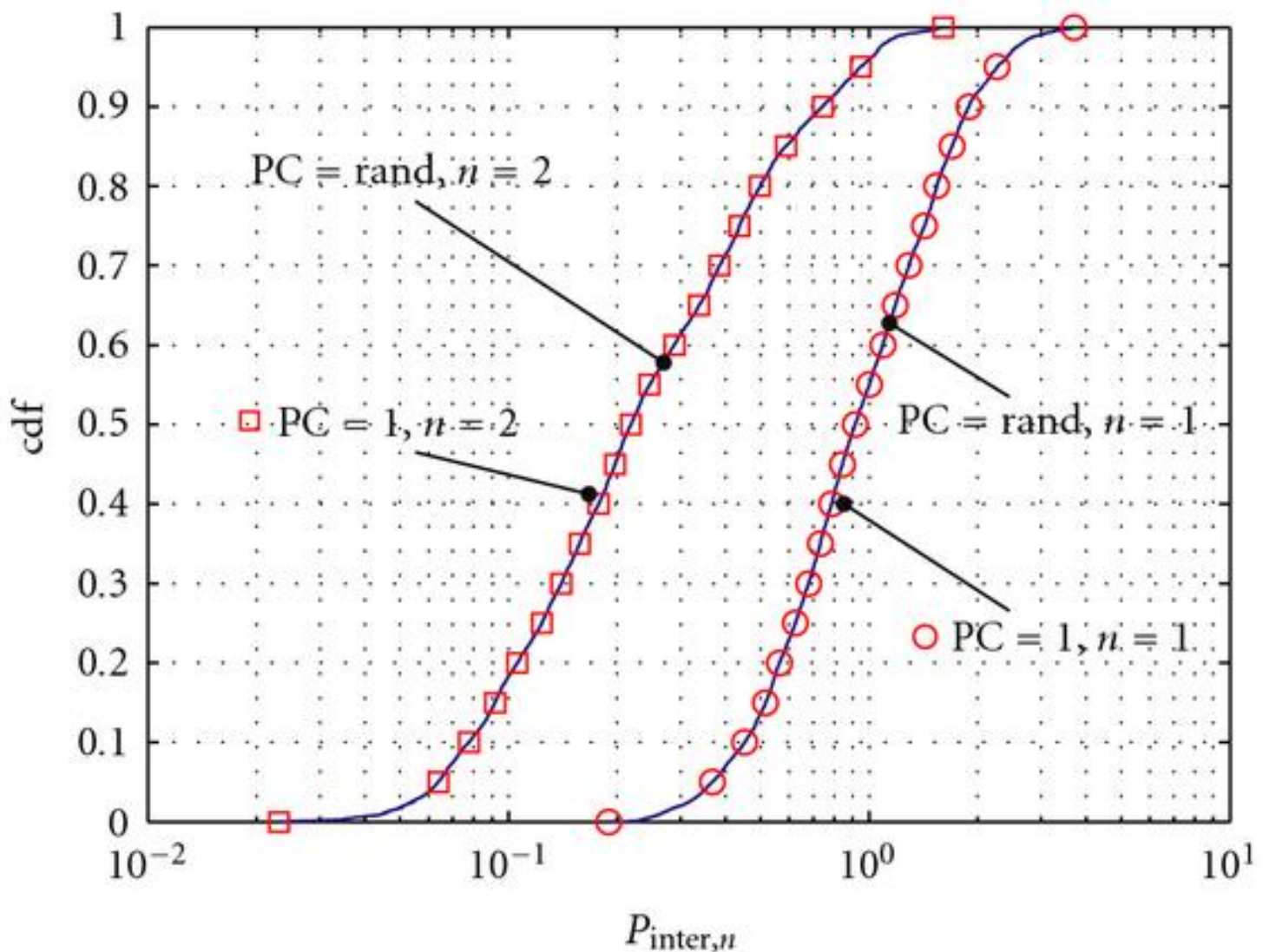
3.2.5. Thermal Noise

We model the thermal noise white and Gaussian, statistically independent and with identical power on all antennas and over all chips that enter the equalizer. Accordingly, we can calculate the power (on symbol level) of the thermal noise as

$$W = \mathbf{E}\left[\| \mathbf{w}_n^T \mathbf{n}_E(k) \|_2^2\right] = \sigma_n^2 \| \mathbf{w}_n^T \|_2^2 . \tag{17}$$

3.3. Fading Parameter Generation

To assess the characteristics of the fading parameter representation, we performed a set of simulations to statistically evaluate the defined parameters. We implemented a fading simulator where the MIMO channel coefficients were generated according to the improved Zheng Model, see [33, 34]. The MMSE equalizer weights and the precoding coefficients were determined assuming perfect channel knowledge at the receiver. Note that the precoding coefficients were chosen according to [1]

$$
\begin{aligned}
w_1 &= w_3 = \frac{1}{\sqrt{2}}, \\
w_2 &\in \left\{ \frac{1+j}{2}, \frac{1-j}{2}, \frac{-1+j}{2}, \frac{-1-j}{2} \right\}, \\
w_4 &= -w_2 .
\end{aligned}
\tag{18}
$$

Accordingly, the precoding is fully determined by the choice of the mobile regarding weight w_2, which was obtained by

$$(w_2)_i = \arg \max_{i=1,\ldots,4} \mathbf{d}_i^H \mathbf{R} \mathbf{d}_i, \tag{19}$$

where $\mathbf{d}_i$ denotes the prefiltering vector of stream one, given by the first column of prefiltering matrix $\mathbf{D}_i = [w_1, w_2, w_3, w_4]$, specified by the value of w_2 subindexed by i. The matrix $\mathbf{R}$ is defined as $\mathbf{R} \triangleq \sum_{n=1}^{n_R} \mathbf{H}_n^H \mathbf{H}_n$, with $\mathbf{H}_n$ denoting the $L \times n_T$ channel matrix, associated to receive antenna n. The intracell power as well as the intercell power are normalized to one at the receiver. The equalizer span and delay were chosen 30 and 15 chips, respectively. Furthermore, we implemented a realistic pre-coding delay of three slots.

Figure 5 shows the fading simulation cdfs of the single stream mode in case of an ITU PedA profile, for the 2×1 MIMO channel. The speed of the mobile was set to 3 km/h. The high values of

the beamforming fading parameter σ_{BF} denote a large gain due to the precoding and small values of the intracell fading parameter σ_{intra} show that the intracell interference can be effectively suppressed by the equalizer. High values of the intercell fading parameter are due to the power normalization as mentioned before (in the system-level simulation, G_{inter} would be weighted with a larger pathloss compared to G_s).

Figure 5 cdfs of the equivalent fading processes for the closed-loop single-stream D-TxAA mode in the 2×1 MIMO case for an ITU PedA channel.
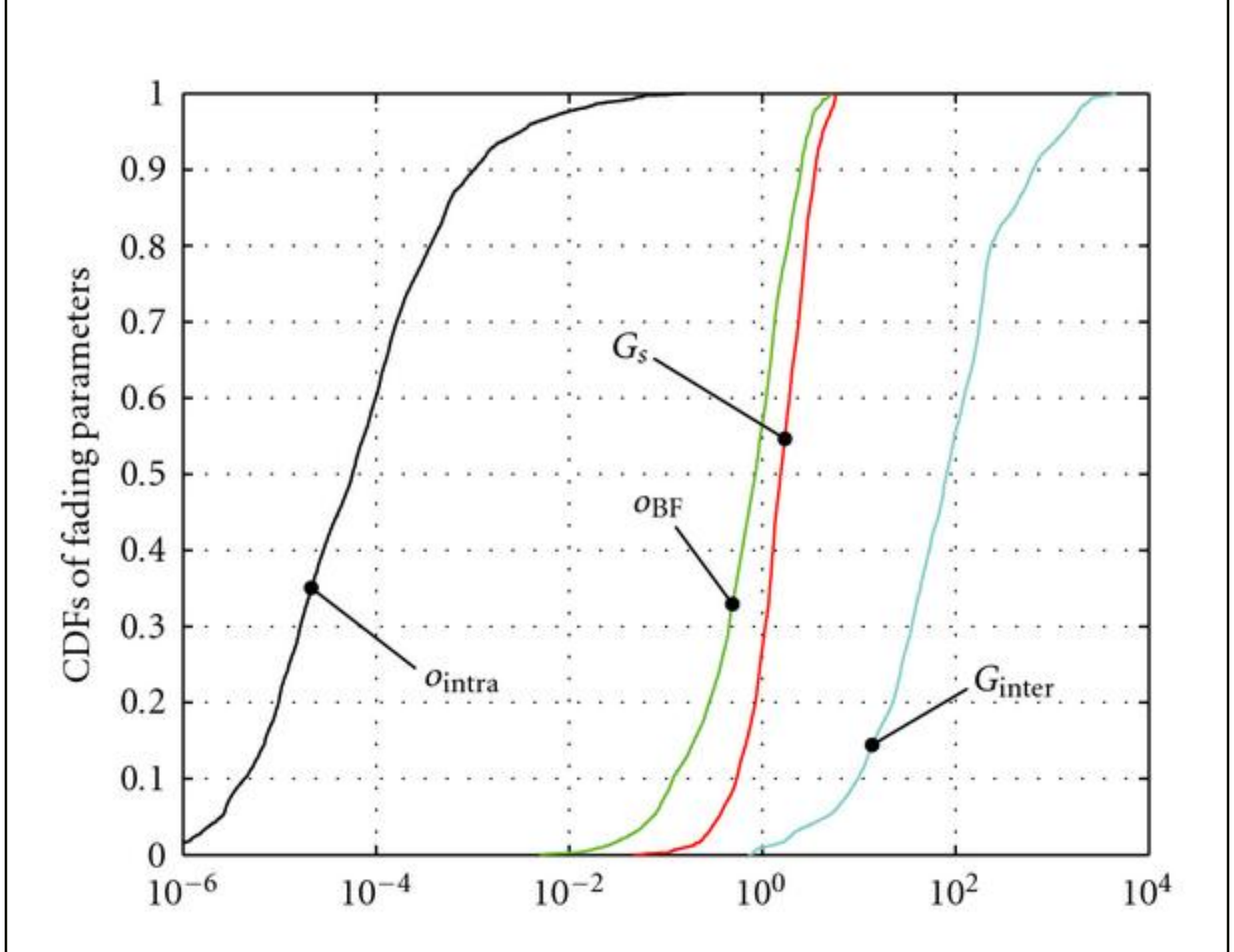

Figure 6 then shows that the results (cdfs again) for the double stream mode in case of an ITU PedA profile 2×2 MIMO channel where the speed of the mobile was again set to 3 km/h. Here, the solid lines denote the equivalent fading processes of the first stream, and the dashed lines illustrate the processes of the second one. The cdfs of the equivalent fading processes of the two streams are separated due to the pre-coding. As defined in (19), the first stream is always preferred in terms of the precoding coefficient evaluation which leads to better statistics in terms of the equivalent fading processes. Another interesting observation is that the beamforming

orthogonality $o_{BF,n} = 1$ is constant in this simulation setup. This can be explained by the fact that in a 2×2 system, only two degrees of freedom exist to separate users by the choice of the precoding vectors. In the double stream mode, however, both degrees of freedom are used for the transmission of the two streams, such that the users do not gain anymore from a possible different choice of their corresponding precoding weights. To be specific, this can be deduced from the following lemma.

Figure 6 cdfs of the equivalent fading processes for the closed-loop double-stream D-TxAA mode in case of an ITU PedA 2×2 MIMO channel.
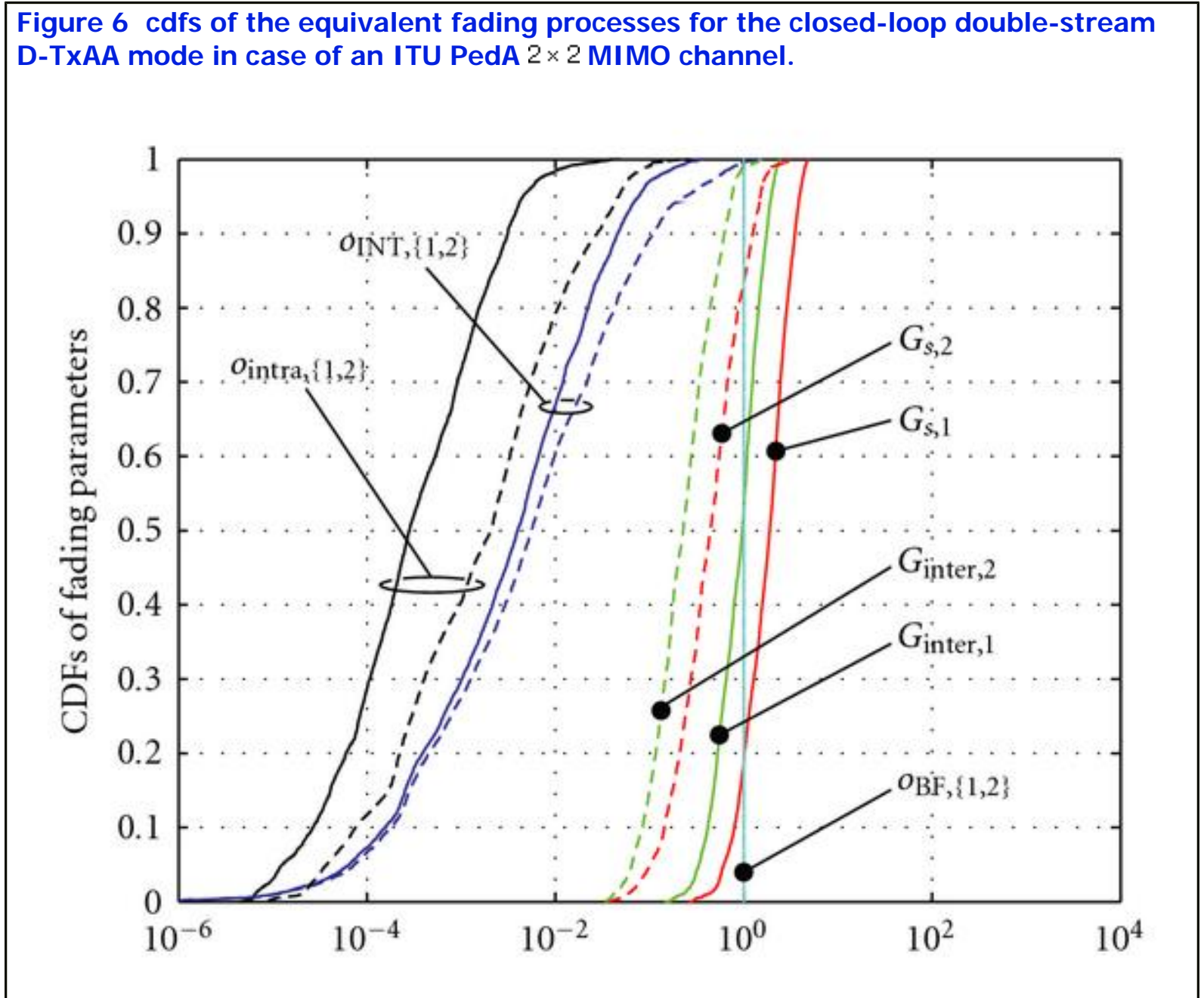
Lemma 1.

Assume that $N = n_T = 2$ and the precoding matrix $\mathbf{D}$ is unitary (which is the case if the precoding coefficients are normalized, see Section 3.3). Then the user index-dependent beamforming orthogonality $o_{BF,u,n}$ is identical to one. In particular, this holds for the averaged beamforming

orthogonality $o_{BF,n}$.

Proof.

The proof is provided in the Appendix.

Figure 7 finally shows the results (cdfs) for the double stream mode in case of an ITU VehA profile in a 2×2 MIMO channel, and a mobile speed of 120 km/h. It can be observed that the performance of the two streams now is nearly equal, which is a result of the precoding delay. The higher Doppler spread leads to a larger mismatch of the determined beamforming weights with the actual MMSE weights, and thus the two streams perform nearly equivalent.

Figure 7 cdfs of the equivalent fading processes for the closed-loop double-stream D-TxAA mode in case of an ITU VehA 2×2 MIMO channel.
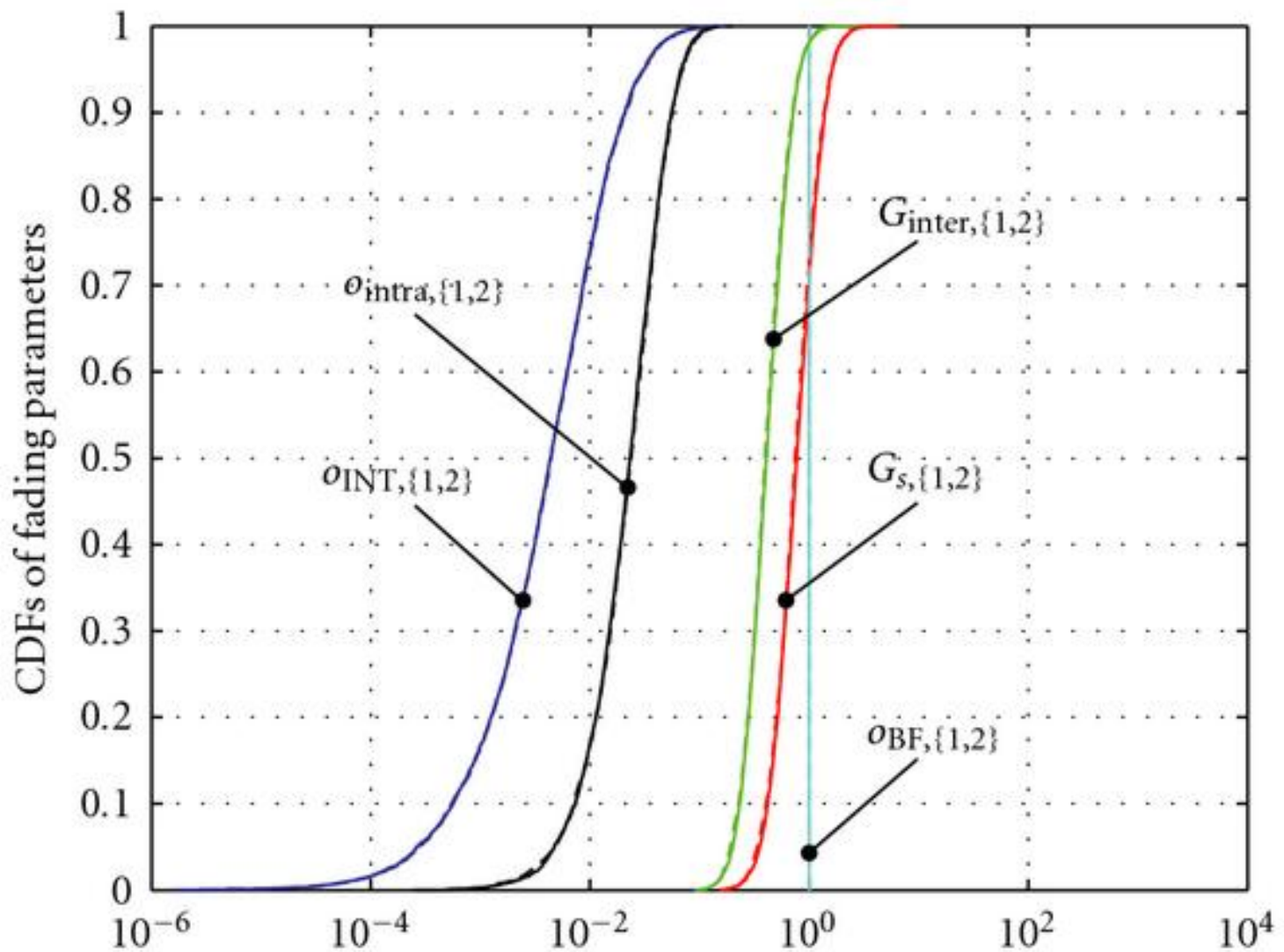
We also investigated the possibility of a direct statistical representation of the fading parameters by means of normal distributed random processes. The form of (6) might suggest this, but the proposed fading parameters show significant deviations from suitable fitted normal random processes. This is due to the nonidentical distribution of the underlying random processes and the correlation between the parameters. As an example, a probability plot of the interstream interference fading parameter $o_{INT,n}$ of stream one is plotted in Figure 8.

Figure 8 Comparison of $o_{INT,n}$ of stream one against a normal distribution.
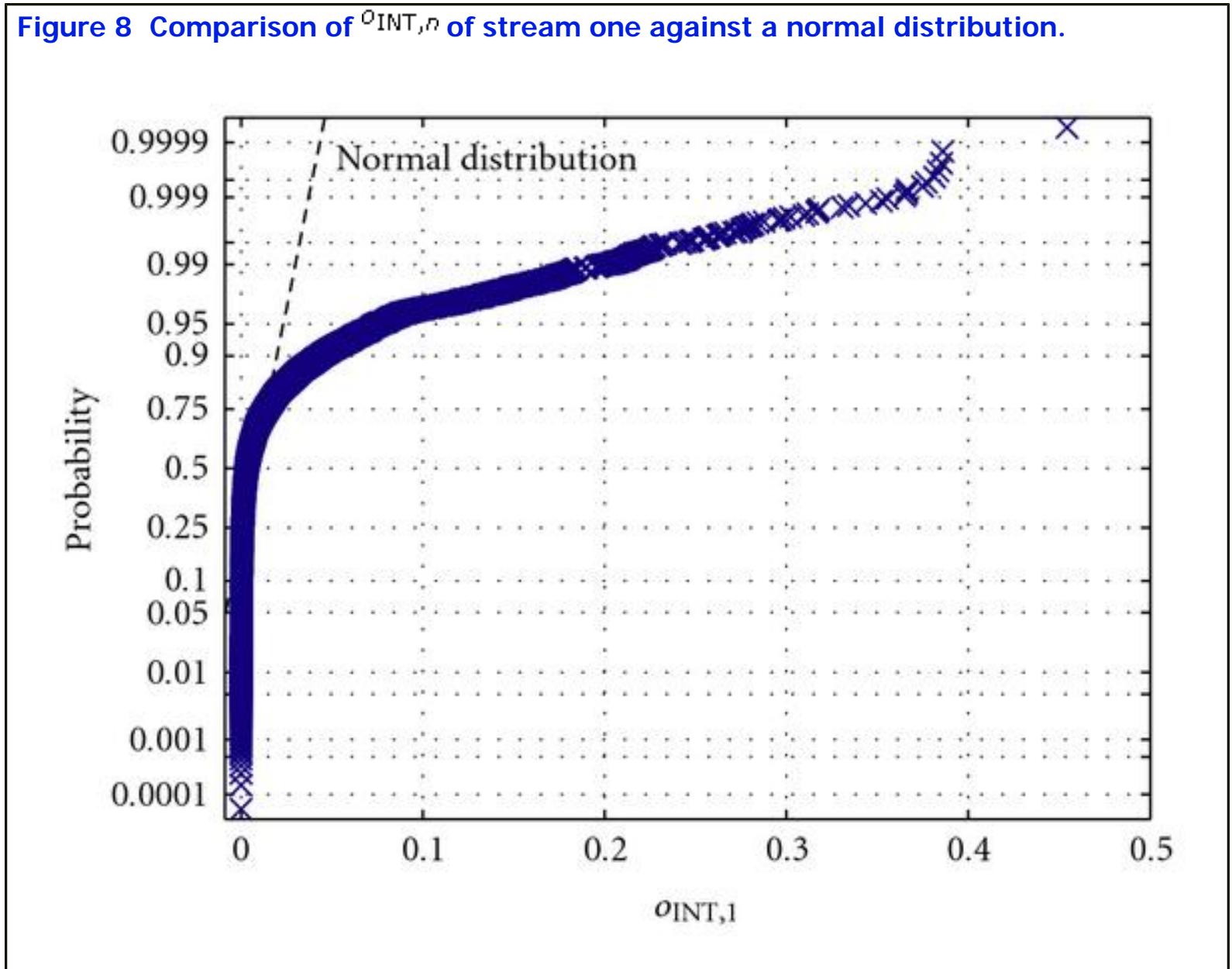
Furthermore, it has to be noted that a statistical representation of the proposed fading parameters would introduce additional losses in accuracy but lead to no (or insignificant) gains in terms of computational complexity.

3.4. Influence of Non-Data Channels

So far we have considered only the effects of the data channel—the so-called High-Speed Downlink Shared CHannel (HS-DSCH)—of HSDPA, but in a network also synchronization and pilot channels are needed [35]. In the context of our modeling, the additional interference imposed by these channels can be split into non-spread channels , for example, the synchronization channels, and the spread channels, for example, the Common Pilot CHannel (CPICH).

For non-spread channels, the additionally imposed interference can—in analogy to the derivations in Section 3.2—be split into three separate parts. Considering the total transmit power of the nonspread channels to be $P_{non\text{-}spread}$, the interference power directly affecting the desired stream n (for which the SINR shall be calculated) is given by $P_{ns,n,1} = G_{s,n} 1 / N P_{non\text{-}spread}$. The interference power added on top of all other transmitted streams is given by

$$P_{ns,n,2} = \sum_{\substack{m=0 \\ m \neq n}}^{N-1} G_{s,n} O_{INT,m} \frac{1}{N} P_{non\text{-}spread},$$
(20)

and the remaining intersymbol and intercode interference can be evaluated to be $P_{ns,n,3} = O_{intra,n} G_{s,n} P_{non\text{-}spread}$. Adding these individual parts, the total interference caused by non-spread channels is given by

$$P_{ns,n} = \sum_{i=1}^{3} P_{ns,n,i} =$$

$$\frac{P_{non\text{-}spread}}{N} G_{s,n} \left[1 + \sum_{\substack{m=0 \\ m \neq n}}^{N-1} O_{INT,m} \right] + P_{non\text{-}spread} O_{intra,n} G_{s,n} \cdot$$
(21)

The interference caused by other spread channels than the HS-DSCH can be treated similarly to the intracell interference caused by loss of spreading code orthogonality. Assuming the total power of other spread channels in the cell to be $P_{other\text{-}spread}$, the interference caused can be evaluated to be

$$P_{s,n} = P_{other\text{-}spread} O_{intra,n} G_{s,n} \cdot$$
(22)

3.5. Resulting SINR Description

With these findings, the SINR on substream n and spreading code ζ, as observed after equalization and despreading (thus on symbol level), can easily be expressed by

$$SINR_{n,\zeta} = \frac{SF \cdot P_{s,n}}{SF \cdot P_{INT,n} + P_{intra,n} + P_{ns,n} + P_{s,n} + P_{inter,n} + W} , \tag{23}$$

where SF denotes the spreading factor. For D-TxAA, in particular, $P_{INT,n}$ simplifies to $P_{INT,n} = O_{INT} \cdot G_{s,n} \cdot P_{m,\zeta}$, since there is only one interfering parallel substream.

The description only contains equivalent fading parameters and power terms, which do not depend on each other. Accordingly, traces for the fading parameters may be generated prior to the system-level simulation—and thus only scalar multiplications will occur in (23) when evaluated on system level. It is also worth noting that in principle only one trace for each fading parameter has to be generated—statistical independency between different realizations for different users can always be achieved by choosing independent starting indices (e.g., drawn uniformly) within the traces. Furthermore, although we only investigated the statistics in case of ITU channel profiles, we want to point out that the proposed structure can be utilized for arbitrary channel models like the Spatial Channel Model (SCM) [36].

3.6. Validation of the Proposed SINR Description

To show that our proposed link-measurement model can accurately approximate the exact SINR, we performed a set of link-level simulations. Figure 9 depicts the simulation results for an ITU PedB channel when an equalizer of length $E = 30$ and 15 spreading codes are employed. The "simulated" or "true" post equalization and despreading SINR is given by

Figure 9 Exemplary model fitting for an equalizer length of 30 and ITU PedB channels, 15 spreading codes employed.
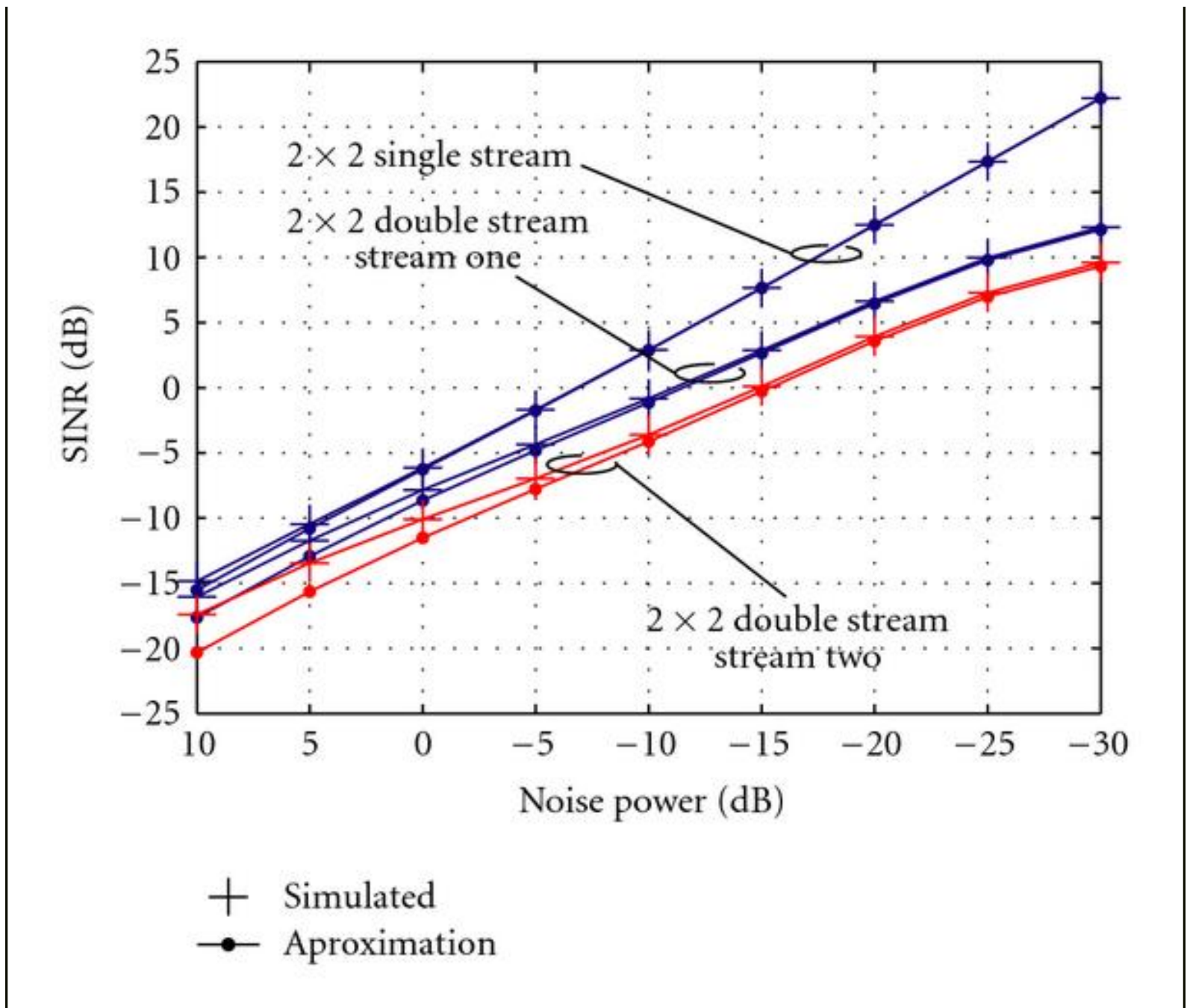
$$SINR_n = \frac{\| s_n \|_2^2}{\| \tilde{s}_n - s_n \|_2^2} , \tag{24}$$

where s_n and $\tilde{s}_n$ denote the transmitted and received symbols on stream n, respectively.

From Figure 9, it can be observed that our proposed model fits the "true" SINR over a large range of noise power. In the single-stream transmission, the SINR increases nearly linear with decreasing noise power, whereas in the double-stream case, interference due to loss of orthogonality between the individual spreading codes leads to a saturation of the SINR. We also conducted investigations in a measurement setup [37], which also showed very good agreement

of the model approximation with the "true" SINR.

3.7. Computational Complexity

To assess the gains in terms of computational complexity of our proposed link-measurement model, we investigated it both analytically and by means of simulations. As already mentioned in Section 3.5 the resulting description of the SINR only requires the loading of the precomputed fading parameters and a couple of real-valued scalar multiplications.

In contrast to that a full evaluation of the SINR without introducing the fading-parameter structure would lead to a large effort in calculating not only the interference terms but also to evaluate the precoding choices and the equalizer coefficients. The computational complexity of the standard SINR calculation can thus be estimated by evaluating these three terms. For the precoding, we base our analysis on (19) for which we obtain

$$\arg \max_{i=1,\ldots,4} \mathbf{d}_i^H \mathbf{R} \mathbf{d}_i \sim 4 \cdot \mathcal{O}\left\{ Ln_T^2 + n_T^2 N + n_T N^2 \right\}, \tag{25}$$

if we assume matrix multiplications to be of order $\mathcal{O}\{k^3\}$ for $k \times k$ matrices. Similarly, the complexity of the equalizer evaluation can be approximated by

$$\mathbf{W}_d = \mathbf{R}_{\mathbf{x}_E \mathbf{x}_E} \Gamma_E^H \left(\Gamma_E \mathbf{R}_{\mathbf{x}_E \mathbf{x}_E} \Gamma_E^H + \mathbf{R}_{\mathbf{n}_E \mathbf{n}_E} \right)^{-1}$$
$$\sim \mathcal{O}\left\{ N^3(E+L-1) + N^3(E+L-1)^2 \right\} \tag{26}$$
$$+ \mathcal{O}\left\{ N^2(E+L-1)n_R E + N^3 n_R^3 E^3 \right\}.$$

Finally, the complexity of the interference power calculation is proportional to

$$\mathcal{O}\left\{ (n_R E + 1)[3 + U_0 N(E+L-2) + BN(E+L-1)] \right\}. \tag{27}$$

Example 1.

If we evaluate this for the double stream case in a 2×2 channel with the length of the channel being $L = 3$ (corresponding to an ITU PedA channel, when the sampling is done on a per slot basis), a maximum of four user to be scheduled in parallel $U_0 = 4$ and only one interfering base station $B = 1$, the complexity of the classical SINR estimation on system level would be expected

to be

$$\mathcal{O}\left\{159 + 72E + 28E^2 + 64E^3\right\}. \tag{28}$$

On the other hand, assuming the computation of the fading parameters is performed offline, the complexity on system level utilizing the proposed structure would result in

$$\mathcal{O}\{N(4 + 2U_0 + B)\}, \tag{29}$$

which is significantly smaller than the complexity order in (28). If the same values as in the previous example are applied, the complexity of the proposed model compared to the complexity of the classical SINR estimation for an equalizer of length $E = 30$ would in this example be $1.48 \cdot 10^{-5}$, however, not considering any memory loading effects.

To verify these large gains in a practical setting, we compared the simulation runtimes of the two approaches in a MATLAB environment. Figure 10 shows the relative complexity of the proposed model compared to the standard approach, defined as

**Figure 10 Average computational time savings in a MATLAB-based simulation for a 2×2 ITU PedA ($L = 3$) channel.**
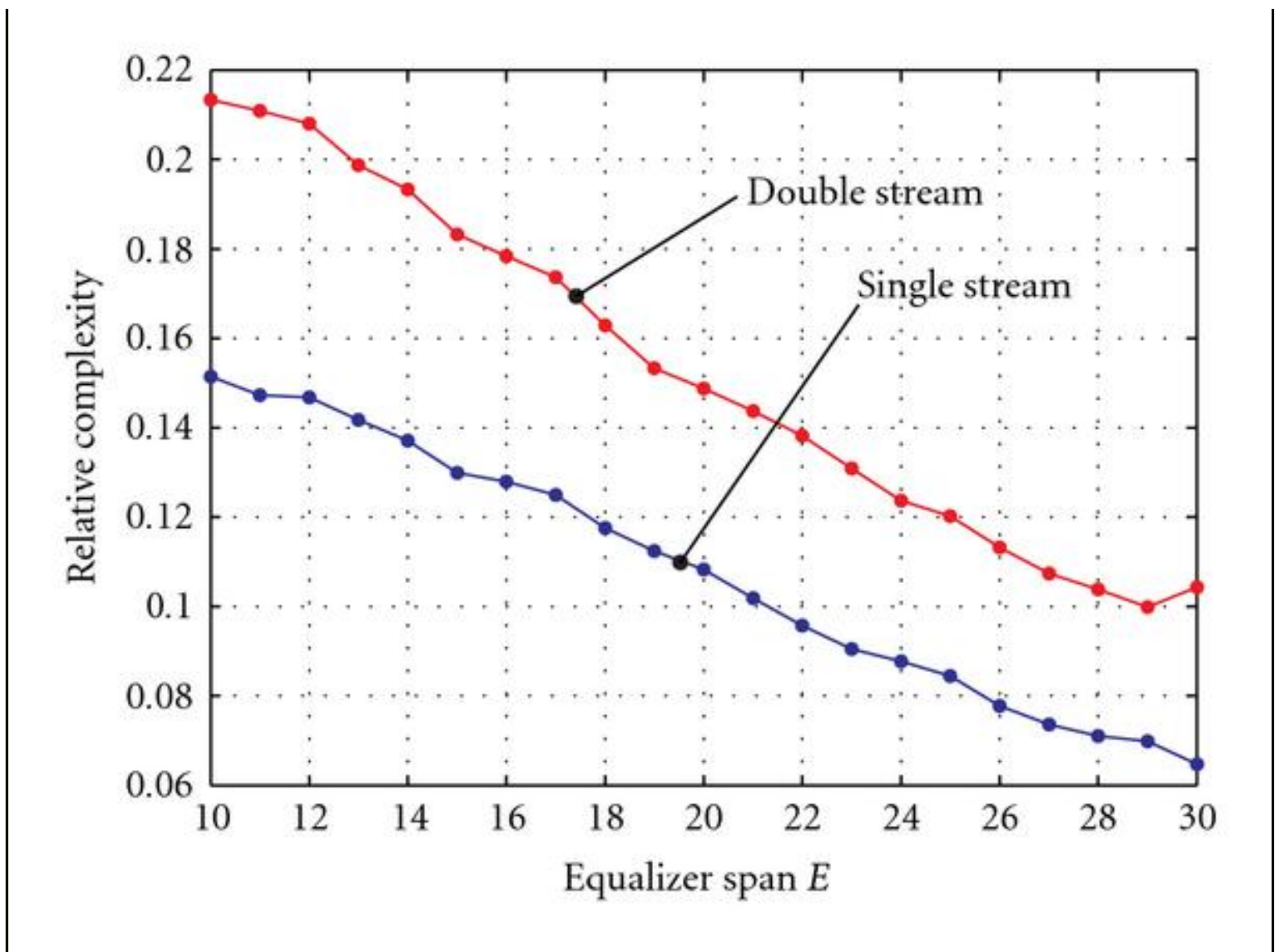
$$g = \frac{t_{proposed}}{t_{classical}}, \tag{30}$$

with $t_{proposed}$ and $t_{classical}$ denoting the time needed to evaluate the SINR with the proposed or the classical model, respectively. It can be observed that our proposed SINR evaluation saves up to 96% of the complexity, depending on the equalizer span E when the same assumptions as in (28) are in place. The reason why the difference is not even more dramatic is because of memory allocation and loading issues in MATLAB that are needed for the operation of the proposed fading parameter approach. Similarly, this effect can be seen when comparing the single-stream and double-stream case, since for the single-stream case, less loading operations have to be conducted, thus leading to larger complexity gains.

4. Link-Performance Model

The basic structure of the proposed link-performance model and its connection to the proposed link-measurement model is depicted in Figure 11. The principal idea follows [22, 23], which we adapted to the needs of the MIMO HSDPA context.

Figure 11 Basic concept of the link-performance model, including the input parameter generation.
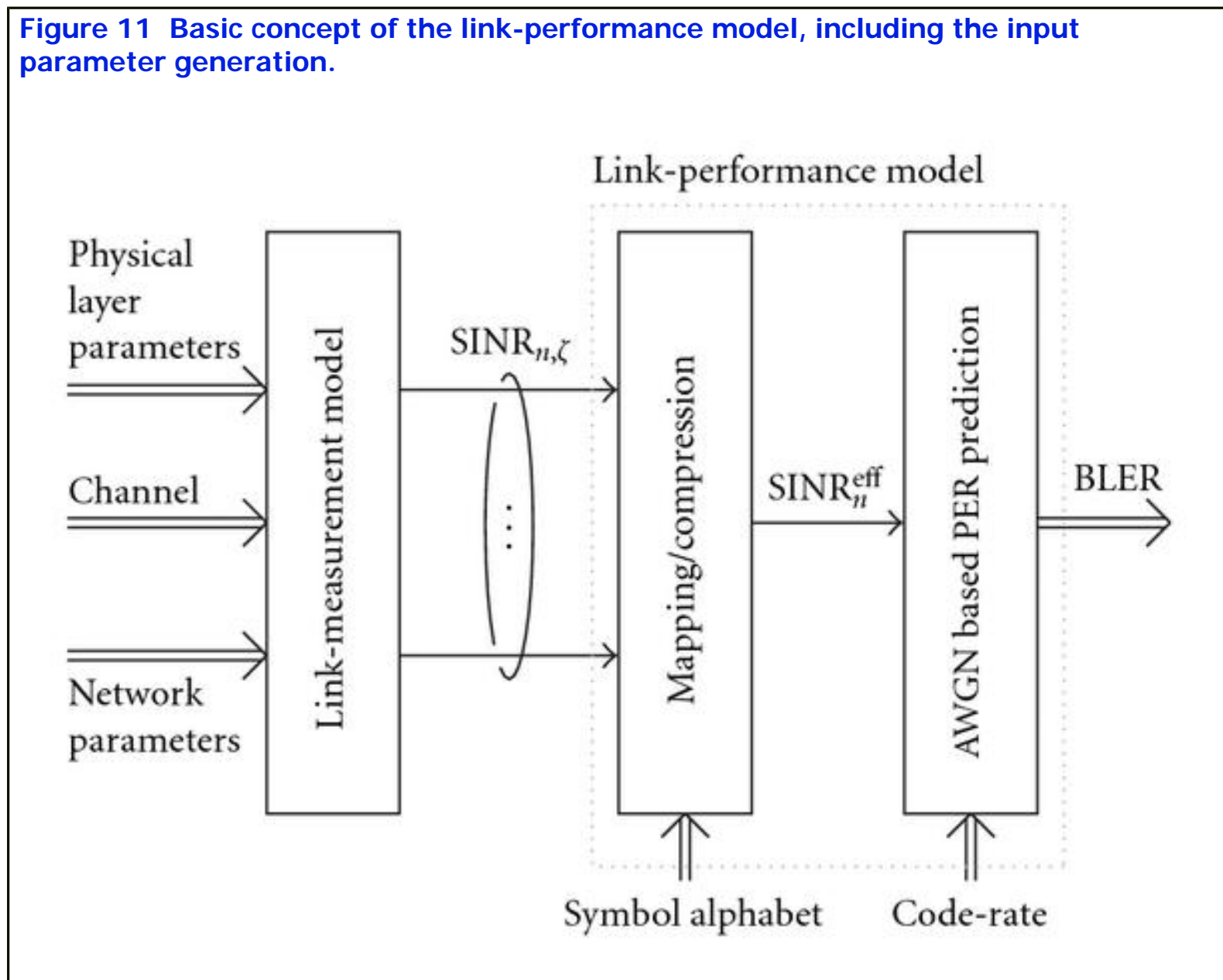
4.1. Mutual Information-Based Averaging

Utilizing the link measurement model, we can compute the SINR per stream and spreading code, $SINR_{n,\zeta}$, from (23). To be able to relate these SINR values to an error event, we have to define a mapping $SINR_{n,\zeta} : \zeta = 1, \dots, |\Phi_{ub}| \mapsto BLER$. We decided in favor of a two-step procedure, mapping the individual SINR values to an *effective* SINR that is able to represent the average quality of the link when the decoder has to deal with the multiplexed data of the

individual spreading codes. In literature, the two most common approaches to perform such a mapping are the Exponential Effective SINR Mapping (EESM) or the Mutual Information Effective SINR Mapping (MIESM). It has been shown that the MIESM in general shows a better performance and is more robust against calibration errors [38]. Accordingly, we decided in favor of the MIESM with a sigmoidal mapping:

$$\text{SINR}_n = \beta \cdot I^{-1}\left(\frac{1}{|\Phi_{ubl}|} \sum_{\zeta=1}^{|\Phi_{ubl}|} I\left(\frac{1}{\beta}\text{SINR}_{n,\zeta}\right)\right), \tag{31}$$

where $I(\cdot)$ is the bit-interleaved coded modulation capacity mapping [23]. The use of the mutual information also appears attractive in the sense that it at least conceptually accounts for the choice of the modulation alphabet. Since the mapping function $I(\cdot)$ is not trivial to be evaluated, we precalculated and stored it in a file that serves as a lookup table during the runtime of the system-level simulation.

The *fitting* parameter β was found by least squares- (LS-) based fitting of the instantaneous symbol-based SINR derived from link-level simulations to the corresponding additive white Gaussian noise (AWGN) performance curves. Details on this approach can be found in [23], however, a full treatment of the training and validation of the model would exceed the scope of this paper. Although our focus in this work is different in terms of the transmission scheme, as well as the targeted channel models, it has to be noted that our resulting tuning parameters are close to the values obtained in [22].

The link-level simulations needed for the training and validation of the link-performance model, as well as for the AWGN performance curves, were obtained by utilizing an HSDPA link-level simulator [39] to compute BLER curves for the SISO AWGN channel. Figure 12 exemplarily shows the postequalization and despreading SINR as well as the AWGN performance curve for a single-stream transmission with settings according to CQI 28 for an UE of capability class 20. It can be observed that the *trained* MIESM maps the postequalization SINR to the AWGN curve with high accuracy.

Figure 12 MIESM training results for a transmission with settings according to CQI 28 in the single-stream operation of a capability class 20 UE.
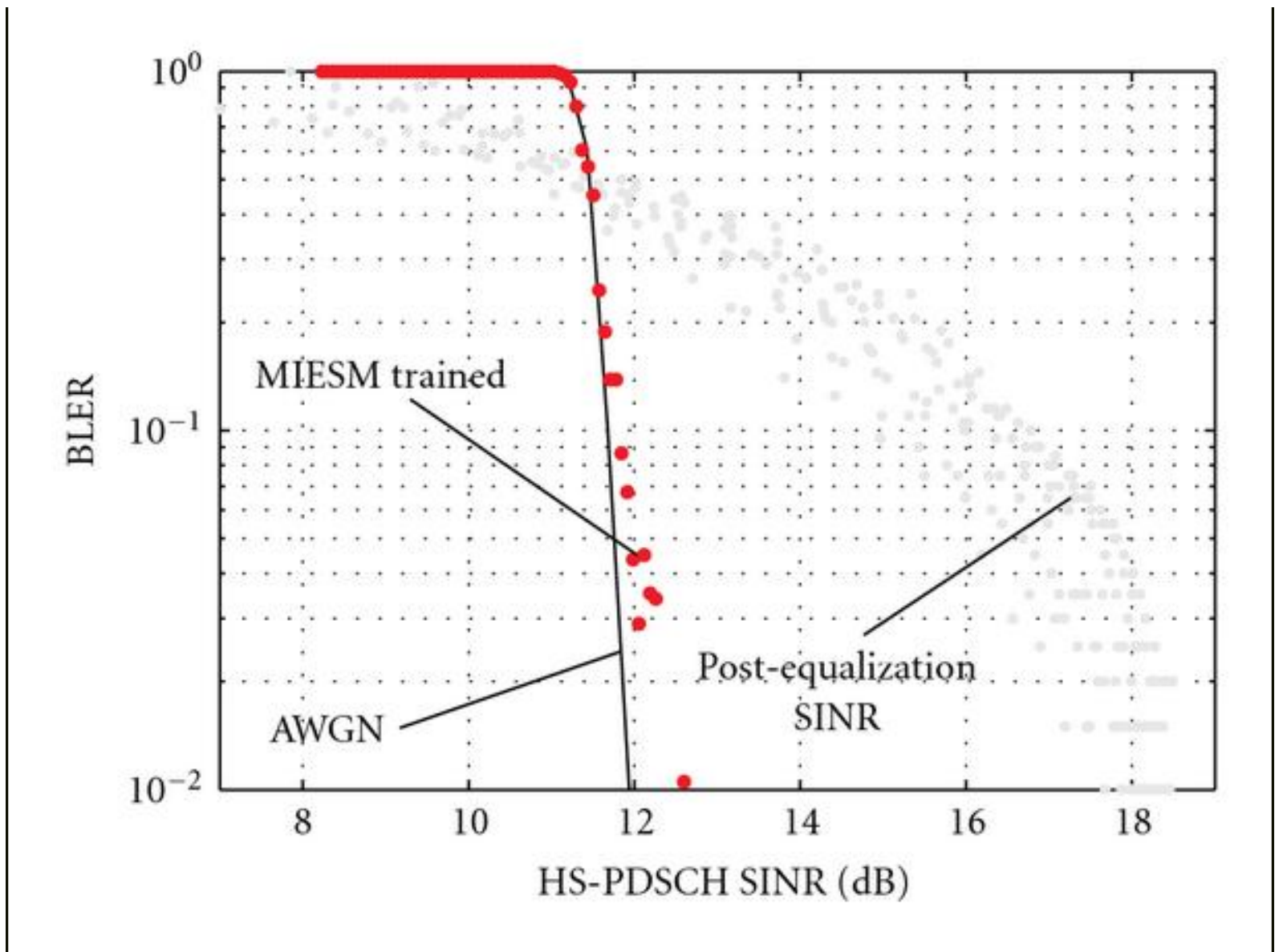
For the desired link-performance model, let us describe the simulated AWGN performance curves by

$$b = f(\text{UE class}, \text{CQI}, n, \text{SINR}_n), \qquad (32)$$

such that the average BLER value corresponding to the effective $\text{SINR}_n^{\text{eff}}$ on stream n can easily be computed by a lookup table. The result then is mapped to a block error event realization by conducting a binary random experiment with probability b for the event of a block error, Non-ACKnowledged (NACK), and probability $1 - b$ for the correct reception of the transport block, ACKnowledged (ACK),

$$\xi = \begin{cases} 0 \rightarrow \mathrm{ACK} & : \Pr(\mathrm{ACK}) = 1 - b, \\ 1 \rightarrow \mathrm{NACK} & : \Pr(\mathrm{NACK}) = b. \end{cases} \tag{33}$$

4.2. SINR-to-CQI Mapping

From the AWGN performance curves needed for the MIESM training, also the mappings for the Adaptive Modulation and Coding (AMC) operation of HSDPA can be extracted [40–42]. If the coherence time of the channel is long compared to the duration of one transmission timing interval, the UE can efficiently utilize the channel with a BLER of approximately 10% by feeding back the adequate CQI values.

4.3. HARQ Gain Modeling

Finally, it remains to specify the modeling of the Hybrid Automatic Repeat reQuest (HARQ) gains in case of retransmissions. In this contribution, we applied a model developed by Frederiksen and Kolding [43], defining the combined SINR after r retransmissions by the recursive equation

$$\left(\mathrm{SINR}_n^{\mathrm{eff}}\right)_r = \epsilon^{r-1} \eta(\mathrm{ECR}, M)_r \cdot \sum_{k=1}^{r} \left(\mathrm{SINR}_n^{\mathrm{eff}}\right)_k, \tag{34}$$

where M is the modulation order and ECR is the code-rate of the first (initial) transmission. The parameter ϵ describes the chase combining efficiency and $\eta(\mathrm{ECR}, M)_r$ is the incremental redundancy gain over chase combining for the rth transmission.

The combined SINR after r retransmissions, $(\mathrm{SINR}_n^{\mathrm{eff}})_r$, can then again be used in the BLER mapping (32) of Section 4.2 to evaluate whether the transport block was received correctly or not.
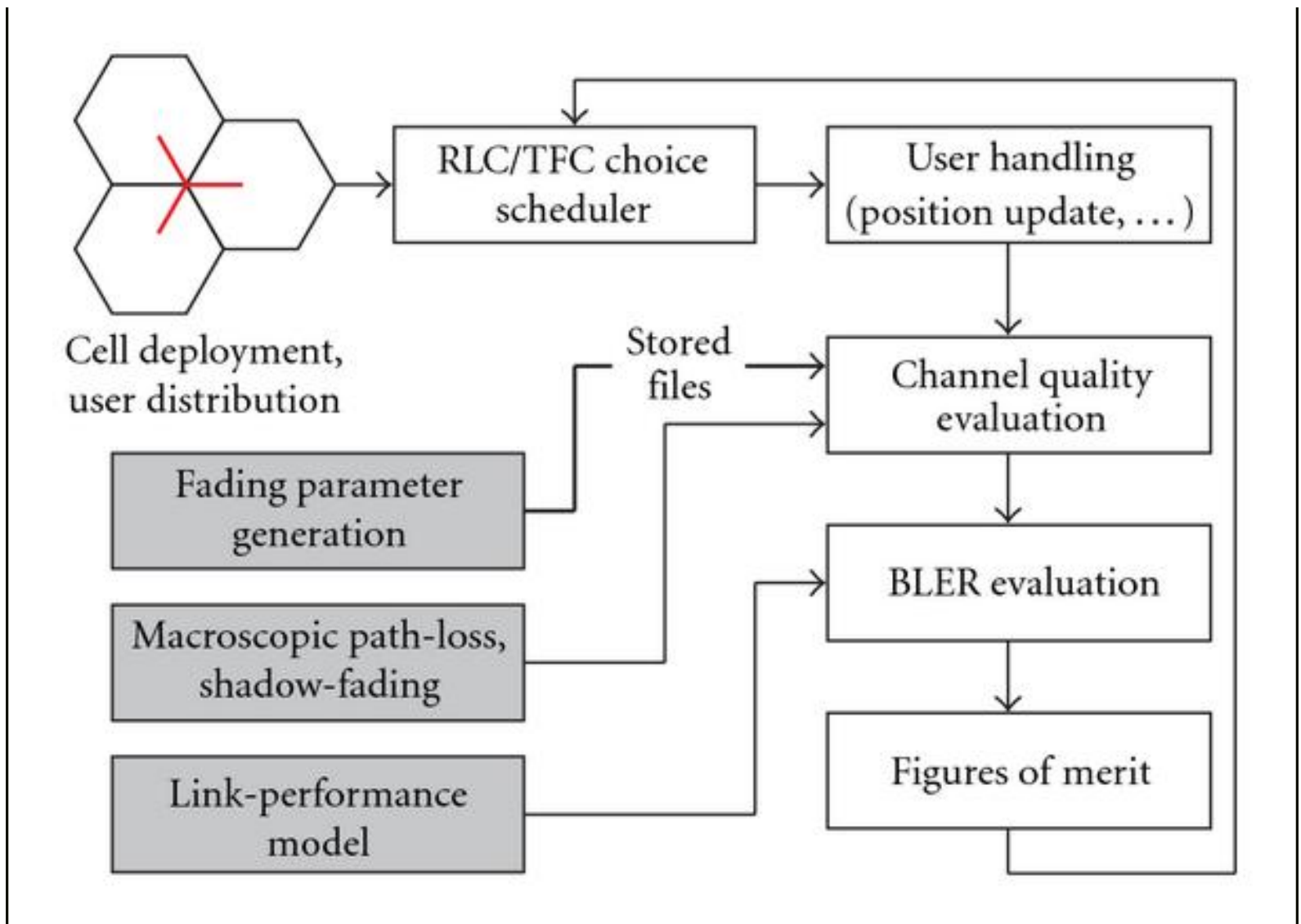
5. System-Level Simulation

System-level simulations are important for a large number of research topics, like network algorithm testing, equipment development, network planning, or even performance testing. Major manufacturers of mobile communication equipment, like Nokia Siemens Networks, Motorola, or Ericsson thus operate their own system-level simulators to derive important results for the standardization process of 3GPP. To show the applicability of the proposed link-to-system level model, we will shortly elaborate on a possible structure of a system-level simulator utilizable for

network performance testing and algorithm optimization, for example, [44, 45], and even for crosslayer topics [46–48].

An overview of the system-level simulation methodology based on the proposed model is illustrated in Figure 13. The first step of the simulation invokes the network generation, that is, cell deployment and the user generation according to the selected UE capability class together with the positioning. Also, the fading parameters suitable for the scenario are loaded, the shadow fading traces are generated and the data necessary for the link-performance model is loaded. In the main simulation loop, according to the feedback of the UE in the target cell, the RLC and the Medium Access Control for HSDPA (MAC-hs) scheduler decide upon the user to be served and the transmission settings of this transmission. After this decision, an update of the user position takes place. With the position being known, the macroscale pathloss, and the effective antenna gain can be calculated. The SINR on each utilized stream and spreading code in the current transmission then is evaluated by (23), mapped to an effective SINR, and consequently the correctness of the received packet is evaluated according to the link-performance model, see (33). The user feedback is then formed of the ACK/NACK report and the CQI for the current transmission evaluated pursuant to the mapping of the UE capability class. At the end of the simulation time, the resulting data is collected and statistically evaluated.

Figure 13 Overview of the system-level simulation methodology, utilizing the proposed fading parameter structure.

According to the structure in Figure 13, the system-level simulator has at least to make some assumptions about the cell deployment, the propagation modeling, and the user mobility scenario. This network layout can, for example, be generated according to live network data or according to regular layouts as described in [36]. Propagation models for system-level simulations then should be chosen to adequately represent the specified deployment scenario. Either measurement data is available, or analytic models, for example, those in [49] can be used. Furthermore, special care should be taken to ensure that the shadow fading obeys the required statistical properties, that is, spatial correlation and intersite correlation, for example, by generation according to [50]. User mobility usually is modeled according to a random walk model, and also more sophisticated path-based test-scenarios can be implemented. Note that depending on the investigation scenario, handover management can be neglected in the simulator, which requires some measures to prevent the users from *leaving* the cell.

Based on the implemented and simulated network scenario, typical performance metrics derived by system-level simulations include cell and user-throughputs, fairness figures, or error statistics.

5.1. Exemplary Simulation Result

An exemplary simulation result of the simulator structure as utilized in [46–48] is illustrated in Figure 14, with the simulation settings specified in Table 1.

Table 1 System-level simulation parameters.

Parameter	Value
Cell deployment	19 cells, layout 1
Node-B distance	1000 m
Transmitter frequency	1.9 GHz
Total power available at Node-B	20 W
CPICH power	0.8 W
Spreading codes available for HS-DSCH	15
Macroscale pathloss model	urban micro [49]
Scheduler	round robin
Active users in target sector	25
User mobility	3 km/h, random direction
UE capability class	20, ST-MMSE equalizer
Equalizer	$E = 30$ chips, $d = 15$ chips
Feedback delay	11 slots

Figure 14 Throughput comparison of different network types and channel conditions.
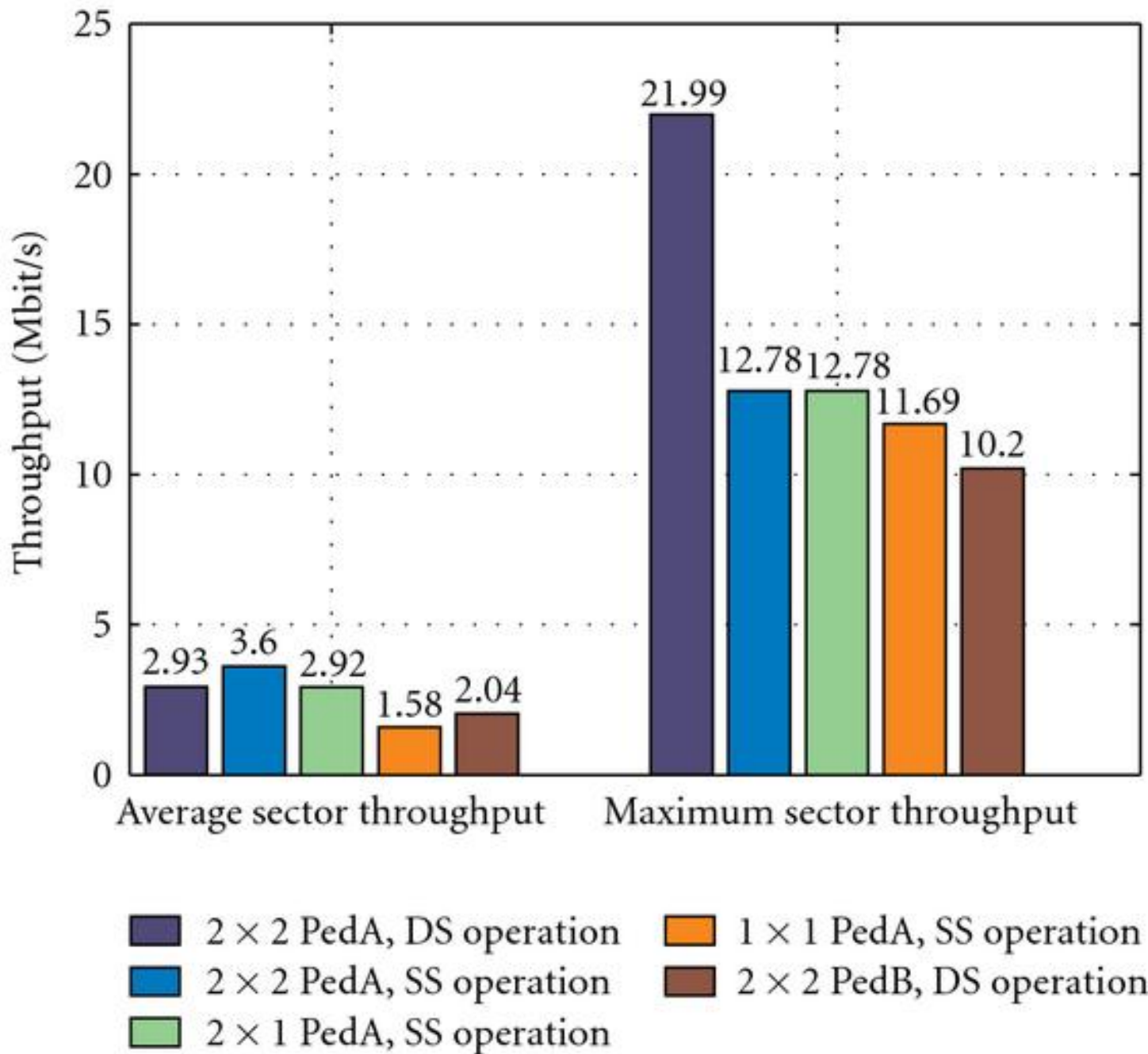
It is noteworthy that the 2×2 double-stream (DS) operation performs slightly worse in the average cell throughput sense than the 2×2 single-stream (SS) transmission. This is an effect of the higher overhead of the dynamic switching between SS and DS mode. Nevertheless, the maximum achievable throughput is significantly larger in the DS enhanced case. A more detailed investigation of the system-level characteristics of MIMO HSDPA will be part of another publication, also elaborating on optimization potential in the network algorithms.

6. Conclusion

In this paper, we introduced a computationally efficient link-to-system level model that includes the precoding, spreading/despreading, and ST-MMSE equalization. Furthermore, we introduced a suitable link-performance mapping scheme and the necessary training to achieve an accurate TTI-based BLER prediction. Together with the necessary SINR-to-CQI mapping and the HARQ modeling, we were able to describe an exemplary implementation of the proposed model in a MATLAB-based system-level simulator and presented details on our simulation methodology.

The introduced model can be utilized for various system-level simulation concepts, network performance investigations, algorithm development, and cross-layer optimizations. Future work based on this link-to-system model will focus on scheduling and interference mitigation techniques, as well as content aware cross-layer techniques.

BodyRef		
FileRef	:	BodyRef/PDF/13638_2009_Article_1651.pdf
TargetType	:	OnlinePDF

Acknowledgments

Appendix

Proof of Lemma 1

Obviously it suffices to show the assertion for $o_{BF,u,n}$. Let us first consider the simpler sum $\sum_{m=0}^{N(E+L-1)-1} |\mathbf{w}_n^T \boldsymbol{\gamma}_{u0}^m|^2$. In fact, this expression equals $\|\mathbf{w}_n^T \Gamma_E\|^2$, where Γ_E is the stacked equivalent channel matrix and $\|\cdot\|$ denotes the norm of a vector in any $\mathbb{C}^l$, $l \in \mathbb{N}$. Since $\Gamma_E = \mathbf{H}_E \cdot (\mathbf{I}_{E+L-1} \otimes \mathbf{D})$, where $\mathbf{D}$ is the precoding matrix of the user u, we obtain by expressing the norm using the scalar product:

$$\sum_{m=0}^{N(E+L-1)-1} \left| \mathbf{w}_n^T \Upsilon_{u0}^m \right|^2$$

$$= \| \mathbf{w}_n^T \Gamma_E \|^2 = \mathbf{w}_n^T \Gamma_E \Gamma_E^H \mathbf{w}_n^* \tag{A1}$$

$$= \mathbf{w}_n^T \mathbf{H}_E (\mathbf{I}_{E+L-1} \otimes \mathbf{D})(\mathbf{I}_{E+L-1} \otimes \mathbf{D}^H) \mathbf{H}_E^H \mathbf{w}_n^*$$

$$= \mathbf{w}_n^T \mathbf{H}_E (\mathbf{I}_{E+L-1} \otimes \mathbf{D}\mathbf{D}^H) \mathbf{H}_E^H \mathbf{w}_n^* .$$

However, by assumption, the precoding matrix is unitary. Hence,

$$\sum_{m=0}^{N(E+L-1)-1} \left| \mathbf{w}_n^T \Upsilon_{u0}^m \right|^2 = \| \mathbf{w}_n^T \mathbf{H}_E \|^2, \tag{A2}$$

and this is independent of the precoding matrix $\mathbf{D}$. For an arbitrary matrix $\mathbf{A}$ and some set $\mathcal{I} \subset \mathbb{N}_0$ of indices, let $\Pi_{\mathcal{I}}(\mathbf{A})$ denote the matrix where the columns with indices in $\mathcal{I}$ are deleted. For the particular index, set $[Nd, Nd + N - 1]$, it can be shown rather quickly that $\Pi_{[Nd,Nd+N-1]}(\Gamma_E) = \Pi_{[Nd,Nd+N-1]}(\mathbf{H}_E)(\mathbf{I}_{E+L-2} \otimes \mathbf{D})$, that is, $\Pi_{[Nd,Nd+N-1]}$ preserves the structure of the matrix Γ_E-block matrix times some block diagonal matrix filled with copies of $\mathbf{D}$. Hence, exactly the same calculations as in (A.1) and (A.2) lead to

$$\sum_{\substack{m=0 \\ m \neq [Nd,Nd+N-1]}}^{N(E+L-1)-1} \left| \mathbf{w}_n^T \Upsilon_{u0}^m \right|^2 = \| \mathbf{w}_n^T \Pi_{[Nd,Nd+N-1]}(\Gamma_E) \|^2$$

$$= \| \mathbf{w}_n^T \Pi_{[Nd,Nd+N-1]}(\mathbf{H}_E) \|^2 . \tag{A3}$$

Since this holds for every user index u, one immediately concludes that $\mathcal{O}_{BF,u,n} \equiv 1$.

References

1. Technical Specification Group Radio Access Network : *Multiple-input multiple-output UTRA.* 3rd Generation Partnership Project (3GPP); 2007.

2. Technical Specification Group Radio Access Network : *Physical layer procedures (FDD).* 3rd Generation Partnership Project (3GPP); 2007.

3. Haring L, Chalise BK, Czylwik A: **Dynamic system level simulations of downlink beamforming for UMTS FDD.** *Proceedings of the IEEE Global Telecommunications Conference (GLOBECOM '03), 2003* **1:** 492-496.

4. Czylwik A, Dekorsy A: **System-level performance of antenna arrays in CDMA-based cellular mobile radio systems.** *EURASIP Journal on Applied Signal Processing* 2004,**2004**(9):1308-1320. 10.1155/S111086570440403X

5. Peppas K, Alexiou A, Lazarakis F, Al-Gizawi T, Axiotis DI: **Performance evaluation at the system level of reconfigurable space-time coding techniques for HSDPA.** *EURASIP Journal on Applied Signal Processing* 2005,**2005**(11):1656-1667. 10.1155/ASP.2005.1656

6. Wrulich M, Weiler W, Rupp M: **HSDPA performance in a mixed traffic network.** *Proceedings of the IEEE Vehicular Technology Conference (VTC '08), May 2008* 2056-2060.

7. Nihtila T, Haikola V: **HSDPA MIMO system performance in macro cell network.** *Proceedings of the IEEE Sarnoff Symposium (SARNOFF '08), 2008* 1-4.

8. Pedersen KI, Lootsma TF, Stottrup M, Frederiksen F, Kolding TE, Mogensen PE: **Network performance of mixed traffic on high speed downlink packet access and dedicated channels in WCDMA.** *Proceedings of the 60th IEEE Vehicular Technology Conference (VTC '04), 2004* **6:** 4496-4500.

9. Sai A PR, Furse C: **System level analysis of noise and interference analysis for a MIMO system.** *Proceedings of the IEEE International Symposium on Antennas and Propagation and USNC/URSI National Radio Science Meeting (APS '08), 2008* 1-4.

10. Gkonis P, Kaklamani D, Tsoulos G: **Capacity of WCDMA multicellular networks under different radio resource management strategies.** *Proceedings of the 3rd International Symposium on Wireless Pervasive Computing (ISWPC '08), 2008* 60-64.

11. Castañeda M, Ivrlac MT, Nossek JA, Viering I, Klein A: **On downlink intercell interference in a cellular system.** *Proceedings of the 18th IEEE International Symposium on Personal, Indoor and Mobile Radio Communications (PIMRC '07), 2007* 1-5.

12. Peppas K, Al-Gizawi T, Lazarakis F, Axiotis DI, Moussa A, Alexiou A: **System level evaluation of reconfigurable MIMO techniques enhancements for HSDPA.** *Proceedings of the IEEE Global Telecommunications Conference (GLOBECOM '04), 2004* **5:** 2869-2873.

13. Pollard A, Heikkila MJ: **A system level evaluation of multiple antenna schemes for high speed downlink packet access.** *Proceedings of the 15th IEEE International Symposium on Personal, Indoor and Mobile Radio Communications (PIMRC '04), 2004* **3:** 1732-1735.

14. Shuping C, Huibin L, Jing H, Dong Z, Asimakis K: **Generalized scheduler providing multimedia services over HSDPA.** *Proceedings of the IEEE International Conference on Multimedia and Expo (ICME '07), 2007* 927-930.

15. Skoutas D, Komnakos D, Vouyioukas D, Rouskas A: **Enhanced dedicated channel scheduling optimization in WCDMA.** *Proceedings of the 14th European Wireless Conference (EW '08), 2008* 1-5.

16. Wrulich M, Eder S, Viering I, Rupp M: **Efficient link-to-system level model for MIMO HSDPA.** *Proceedings of the 4th IEEE Broadband Wireless Access Workshop, 2008*

17. Staehle D, Mader A: **A model for time-efficient HSDPA simulations.** *Proceedings of the 66th IEEE Vehicular Technology Conference (VTC '07), 2007* 819-823.

18. Seeger A, Sikora M, Klein A: **Variable orthogonality factor: a simple interface between link and system level simulation for high speed downlink packet access.** *Proceedings of the 58th IEEE Vehicular Technology Conference (VTC '03), September 2003* 2531-2534.

19. Wrulich M, Rupp M: **Efficient link measurement model for system level simulations of Alamouti encoded MIMO HSDPA transmissions.** *Proceedings of the International ITG Workshop on Smart Antennas (WSA '08), February 2008, Darmstadt, Germany* 351-355.

20. Moltchanov D, Koucheryavy Y, Harju J: **Simple, accurate and computationally efficient wireless channel modeling algorithm.** In *Wired/Wireless Internet Communications, Lecture Notes in Computer Science. Volume 3510*. Springer, Berlin, Germany; 2005:234-245. 10.1007/11424505_23

21. Moltchanov D, Koucheryavy Y, Harju J: **Cross-layer modeling of wireless channels for data-link and IP layer performance evaluation.** *Computer Communications* 2006,**29**(7):827-841. 10.1016/j.comcom.2005.08.005

22. Brueninghaus K, Astely D, Salzer T, *et al*.: **Link performance models for system level simulations of broadband radio access systems.** *Proceedings of the 16th IEEE International Symposium on Personal, Indoor and Mobile Radio Communications (PIMRC '05), September 2005* **4:** 2306-2311.

23. Members of WINNER : *Assessment of advanced beamforming and MIMO technologies.* WINNER; 2003.

24. Nihtila T, Kurjenniemi J, Virtej E: **System level analysis of interference aware LMMSE chip equalization in HSDPA network.** *Proceedings of the 12th IEEE Symposium on Computers and Communications (ISCC '07), 2007* 133-138.

25. Mirkovic J, Orfanos G, Reumerman H-J: **MIMO link modeling for system level simulations.** *Proceedings of the 17th IEEE International Symposium on Personal, Indoor and Mobile Radio Communications (PIMRC '06), 2006* 1-6.

26. Wrulich M, Mehlführer C, Rupp M: **Interference aware MMSE equalization for MIMO TxAA.** *Proceedings of the 3rd International Symposium on Communications, Control, and Signal Processing (ISCCSP '08), 2008* 1585-1589.

27. Mehlführer C, Wrulich M, Rupp M: **Intra-cell interference aware equalization for TxAA HSDPA.** *Proceedings of the 3rd International Symposium on Wireless Pervasive Computing (ISWPC '08), 2008* 406-409.

28. Members of 3GPP : *A comparison of ideal relative data throughput of MIMO and release 5.* 3GPP; 2003.

29. Szabo A, Geng N, Seegert A, Utschick W: **Investigations on link system level interface for MIMO systems.** *Proceedings of the 3rd IEEE International Symposium on Image and Signal Processing and Analysis (ISPA '03), September 2003* **1:** 365-369.

30. Kim B-H, Zhang X, Flury M: **Linear MMSE space-time equalizer for MIMO multicode CDMA systems.** *IEEE Transactions on Communications* 2006,**54**(10):1710-1714.

31. Proakis J: *Digital Communications*. 4th edition. McGraw-Hill, Boston, Mass, USA; 2000.

32. Members of ITU : *Recommendation ITU-R M.1225: guidelines for evaluation of radio transmission technologies for IMT-2000.* International Telecommunication Union (ITU); 1997.

33. Zheng YR, Xiao C: **Simulation models with correct statistical properties for rayleigh fading channels.** *IEEE Transactions on Communications* 2003,**51**(6):920-928. 10.1109/TCOMM.2003.813259

34. Zemen T, Mecklenbrauker CF: **Time-variant channel estimation using discrete prolate spheroidal sequences.** *IEEE Transactions on Signal Processing* 2005,**53**(9):3597-3607.

35. Dahlman E, Parkvall S, Skold J, Beming P: *3G Evolution: HSDPA and LTE for Mobile Broadband*. Academic Press, New York, NY, USA; 2007.

36. Technical Specification Group Radio Access Network : *Spatial channel model for multiple input multiple output (MIMO) simulations.* 3rd Generation Partnership Project (3GPP); 2007.

37. Mehlführer C, Caban S, Wrulich M, Rupp M: **Joint throughput optimized CQI and precoding weight calculation for MIMO HSDPA.** *Proceedings of the 42nd Asilomar Conference on Signals, Systems and Computers, October 2008*

38. Cipriano AM, Visoz R, Salzer T: **Calibration issues of PHY layer abstractions for wireless broadband systems.** *Proceedings of the 68th IEEE Vehicular Technology Conference (VTC '08), 2008* 1-5.

39. Kaltenberger F, Freudenthaler K, Paul S, *et al*.: **Throughput enhancement by cancellation of synchronization and pilot channel for UMTS high speed downlink packet access.** *Proceedings of the 6th IEEE Workshop on Signal Processing Advances in Wirless Communications (SPAWC '05), 2005* 580-584.

40. Members of TSG-RAN Working Group 4 : *Revised HSDPA CQI proposal.* 3GPP; 2002.

41. Brouwer F, de Bruin I, Silva J, Souto N, Cercas F, Correia A: **Usage of link-level performance indicators for HSDPA network-level simulations in E-UMTS.** *Proceedings of the 8th IEEE International Symposium on Spread Spectrum Techniques and Applications, 2004* 844-848.

42. Litjens R: **HSDPA flow level performance and the impact of terminal mobility.** *Proceedings of the IEEE Wireless Communications and Networking Conference (WCNC '05), 2005* **3:** 1657-1663.

43. Frederiksen F, Kolding TE: **Performance and modeling of WCDMA/HSDPA transmission/H-ARQ schemes.** *Proceedings of the 56th IEEE Vehicular Technology Conference (VTC '02), 2002* 472-476.

44. Mäder A, Staehle D, Spahn M: **Impact of HSDPA radio resource allocation schemes on the system performance of UMTS networks.** *Proceedings of the 66th IEEE Vehicular Technology Conference (VTC '07), 2007* 315-319.

45. Yan X, Khan J, Jones B: **An adaptive resource management technique for a HSDPA network.** *Proceedings of the IFIP International Conference on Wireless and Optical Communication Networks (WOCN '07), 2007* 1-5.

46. Lilley G, Wrulich M, Rupp M: **Network based stream-number decision for MIMO HSDPA.** *Proceedings of the ITG International Workshop on Smart Antennas (WSA '09), February 2009*

47. Superiori L, Wrulich M, Svoboda P, Rupp M: **Cross-layer optimization of video services over HSDPA networks.** *Proceedings of the ICST International Conference on Mobile Lightweight Wireless Systems, 2009*

48. Superiori L, Wrulich M, Svoboda P, *et al.*: **Content-aware scheduling for video streaming over HSDPA networks.** *Proceedings of the 2nd IEEE International Workshop on Cross-Layer Design, 2009*

49. Cichon DJ, Kürner T: *COST 231—Digital Mobile Radio Towards Future Generation Systems*. COST; 1998.

50. Gudmundson M: **Correlation model for shadow fading in mobile radio systems.** *Electronics Letters* 1991,**27**(23):2145-2146. 10.1049/el:19911328